NASA TN D-972

TECHNICAL NOTE

D-972

EXPERIMENTAL AND THEORETICAL STUDIES OF THE EFFECTS OF CAMBER AND TWIST ON THE AERODYNAMIC CHARACTERISTICS OF PARAWINGS HAVING NOMINAL ASPECT RATIOS OF 3 AND 6

By Edward C. Polhamus and Rodger L. Naeseth

Langley Research Center
Langley Station, Hampton, Va.

NATIONAL AERONAUTICS AND SPACE ADMINISTRATION
WASHINGTON

January 1963

NATIONAL AERONAUTICS AND SPACE ADMINISTRATION

TECHNICAL NOTE D-972

EXPERIMENTAL AND THEORETICAL STUDIES OF THE EFFECTS OF CAMBER AND TWIST ON THE AERODYNAMIC CHARACTERISTICS OF PARAWINGS HAVING NOMINAL ASPECT RATIOS OF 3 AND 6

By Edward C. Polhamus and Rodger L. Naeseth

SUMMARY

Low-speed wind-tunnel studies were made of the effects of camber and twist and the effects of aspect ratio on the aerodynamic characteristics of parawings. To determine the effects of camber and twist, tests were made both with the conventional conical-type canopy, which provides camber and washout, and with a cylindrical-type canopy which provides essentially zero camber and twist. With regard to aspect ratio, tests were made of parawings having aspect ratios of 3 and 6; the range was thereby extended well beyond that of previous investigations. The degree to which airfoil and wing theory can be used to predict the aerodynamic characteristics of parawings was also investigated.

The results indicated large improvements in lift-drag ratio can be obtained both by the use of the cylindrical canopy and by the use of a high-aspect-ratio canopy. The aspect-ratio-6 cylindrical parawing provided a maximum lift-drag ratio of approximately 13.6. The results also indicated that, for conical type canopies, improvements in the zero-lift pitching-moment characteristics could be obtained by use of the higher aspect ratio. With regard to theory the results indicated that sufficient accuracy for preliminary design can be obtained by use of the Pankhurst method for camber effects and the Weissinger method for angle-of-attack and twist effects. The cylindrical canopies loaded up at low angles of attack; thus, these canopies provided a useful range of low lift coefficients not available with the conical surface parawings.

INTRODUCTION

The National Aeronautics and Space Administration is engaged in a research program directed toward various applications of the parawing concept. (See refs. 1 to 10.) To date these studies have been concerned, for the most part, with the use of such flexible wings as part of the recovery systems for space vehicles and rocket boosters. For such uses, only moderate lift-drag ratios are required to provide considerable improvement over parachute systems and provide the

ability to maneuver to a desired landing site. Other possible applications, however, such as lightweight main or auxiliary wings for powered aircraft and for towed fuel or cargo packages, for example, are under consideration in addition to extended-range glide recovery of spacecraft and boosters. These missions place considerable importance on the attainment of improved aerodynamic efficiency.

The canopies of previously investigated parawings assume essentially a conical shape in flight. Streamwise sections of these conical shapes show rather extreme geometric twist distributions that would be expected to result in appreciable losses in the maximum lift-drag ratio. (See fig. 5 of ref. 8, for example.) In addition, because of structural and stowage considerations, low-aspect-ratio planforms have been used and thereby cause a further restriction on the available lift-drag ratio. The present investigation was therefore initiated to obtain an indication of the improvement in aerodynamic efficiency that might be provided by improvements in span-load distribution and planform. The investigation, which was made at low subsonic speeds in the Langley 7- by 10-foot transonic tunnel, included comparisons of conical canopies with canopies having essentially zero twist and camber (cylindrical canopies) for planforms having leading-edge sweep angles of 50° and nominal aspect ratios of 3 and 6.

Inasmuch as the purpose of this investigation was to determine the aerodynamic effects associated with particular changes in canopy shape, rigid leading edges, keels, and spreader bars were used in order that a canopy shape under air load reasonably similar to that desired might more easily be maintained. In many practical applications, of course, it would be desirable to use the results obtained to design less rigid configurations that take greater advantage of the paraglider tension structure concept.

SYMBOLS

The coefficients are presented for the wind system of axes. (See fig. 1.) All moments are given about the 25-percent-chord point of the mean aerodynamic chord of the flat pattern of the canopies and all coefficients are based on the flat pattern area and keel length.

A	aspect ratio, b'^2/S
b	span of deployed parawing, ft
b'	span of flat pattern, ft
c	local wing chord, measured parallel to keel, ft
$\bar{c}$	wing mean aerodynamic chord, $\frac{2}{S}\int_0^{b/2} c^2 dy$, ft
c_{av}	average wing chord, ft

c_k keel length, ft

c_l section lift coefficient, $\frac{\text{Section lift}}{qc}$

c_{l_α} section lift-curve slope per degree

C_D drag coefficient, $\frac{\text{Drag}}{qS}$

C_L lift coefficient, $\frac{\text{Lift}}{qS}$

C_{L_α} wing lift-curve slope per degree

C_m pitching-moment coefficient, $\frac{\text{Pitching moment}}{qSc_k}$

C_{m_o} value of pitching-moment coefficient at $C_L = 0$

L/D lift-drag ratio

$(L/D)_{max}$ maximum lift-drag ratio

q free-stream dynamic pressure, $\frac{\rho V^2}{2}$, lb/sq ft

R radius of basic cylinder, in.

S area of flat pattern, sq ft

V free-stream velocity, ft/sec

x_{ac} distance from leading edge of keel to aerodynamic center, ft

y spanwise distance, ft

$\frac{y}{b/2}$ nondimensional spanwise distance

α angle of attack of keel, deg

$\alpha_{L=0}$ wing or section angle of attack at which lift is zero

ϵ total aerodynamic twist angle between wing root and wing tip, positive for washout at tip, deg

ϵ_{geom}	geometric twist angle between a line connecting leading edge and trailing edge of a section and reference plane containing keel, deg
ϵ_{local}	aerodynamic twist at a particular spanwise station, deg
θ	half-angle of segment of cone assumed for parawing surface
Λ	sweep of deployed leading edge
$\Lambda_{c/4}$	sweep of wing quarter-chord line
λ	taper ratio, $\frac{\text{Tip chord}}{\text{Root chord}}$
ρ	free-stream air density, slugs/cu ft
ϕ	half-angle of basic cone used in calculation of airfoil profiles

MODEL AND APPARATUS

As the first step in the development of a wide range of parawing shapes, tests were made of models which had rigid frames with fabric canopies attached to the rigid leading edges and keel. The canopies were designed to approximate two basic surface forms, each semispan a part of the surface of a cone or of a cylinder. Photographs of these two types are shown in figure 2.

The conical aspect-ratio-2.8 model (fig. 3(a)) is the type of wing most used in previous investigations. In making the model, a nonporous fabric was attached to three equal length members joined at the apex. (The fabric attachment was at the top of the keel and at the nose of the leading edges.) With the cloth stretched tightly and the leading-edge sweep at 45° the members formed the "flat planform." When the sweep was increased to 50° (deployed planform), the fabric became slack. Under airload this fabric supported by a rigid keel and leading edge forms a surface which is best approximated by a cone. The sweep of the trailing edge and the length of the keel were changed to obtain the aspect-ratio-6 conical model. (See fig. 3(b).)

A considerable amount of twist (washout) and camber are characteristics of the conical surfaces and, as a result, these wings have shown modest values of $(L/D)_{max}$ which occur at fairly high lift coefficients. In order to broaden the range of parawing characteristics available for various applications, the camber and twist were reduced to zero by designing the wing semispans to approximate the surface of a cylinder with axes parallel to the airstream. With this design a high $(L/D)_{max}$ was expected while retaining directional stability and the advantages of a tension surface. The aspect-ratio-2.7 and 5.8 models are shown in figures 3(c) and 3(d). The planform was adapted from the aspect-ratio-6 conical model (fig. 3(b)) by maintaining identical positions of the deployed apex and wing tips and the same canopy trailing edge and keel lengths. The trailing edge was assumed to be a helix and the diameter of the cylinder on which it lay was calculated. It was then possible to determine the leading edge as a helix of

different pitch on the same cylinder. Because of the curvature of the cylindrical frame, the cylindrical flat pattern layout differs from the conical flat pattern layout in span and area and, therefore, in aspect ratio. Except in this section of the report, nominal aspect ratios of 3 and 6 are used to simplify reference to the models. The insert on figure 3(d) shows a tip-chord extension which was also tested. The aspect-ratio-2.7 cylindrical surface parawing was constructed by extending the keel length of the aspect-ratio-5.8 model.

The fabric used to form the membranes of all the models consisted of nonporous Mylar film bonded to a nylon ripstop parachute cloth. All membranes were applied with the warp parallel to the trailing edge. Some of the more pertinent geometric characteristics are presented in the following table:

	Geometric characteristics of -			
	Conical-type canopy		Cylindrical-type canopy	
Aspect ratio:				
Flat	2.83	6.00	2.74	5.81
Deployed	2.57	5.45	2.57	5.46
Area, sq ft:				
Flat	12.27	5.79	11.88	5.60
Deployed	11.16	5.26	11.16	5.26
$\bar{c}$, in.:				
Flat	33.33	15.70	33.33	15.70
Deployed	33.33	15.70	33.33	15.70
b, in.:				
Flat	70.71	70.71	68.44	68.44
Deployed	64.28	64.28	64.28	64.28
Root chord, in.:	50.00	23.57	50.00	23.57
Sweep angle, deg:				
Flat	45.00	45.00	48.23	48.23
Deployed	50.00	50.00	*50	*50
Deployed $\frac{1}{4}$ chord	38.80	45.30	38.80	45.30
Deployed $\frac{1}{2}$ chord	22.50	39.50	22.50	39.50

*Average value.

The frame of the aspect-ratio-2.8 conical model (fig. 3(a)) was made of welded 3/4-inch aluminum tubing. The other models had a common spreader bar and

keel. Vertical struts were added to the end of the spreader bar for the cylindrical models to hold the nose, keel, and wing tips in a common plane. The leading edges of the models, except the aspect-ratio-2.8 conical, tapered from 3/4 inch at the apex to 1/4 inch at the tips. As shown in the small cross-section drawings, the conical model leading-edge spars were round and the cylindrical model spars were made up of a half round piece and a rectangular piece.

The models were mounted on a sting-supported six-component strain-gage balance. (See fig. 2.) Measurements were made in the Langley 7- by 10-foot transonic tunnel which utilizes perforated walls in the test section.

TESTS AND CORRECTIONS

The tests were made at dynamic pressures of 5 pounds per square foot for the conical surface models and 8 pounds per square foot for the cylindrical surface models. The conical model was tested at the lower value to keep model deflections small. A less flexible leading edge was used on the cylindrical models. (See cross sections of fig. 3.) The Reynolds numbers based on keel length are given in the following table:

Model	q, lb/sq ft	Reynolds number for nominal aspect ratios of -	
		3	6
Conical	5	1,680,000	820,000
Cylindrical	8	2,120,000	1,030,000

No jet-boundary and blocking corrections were necessary since it has been determined experimentally that, for this size model in the vented test section, such corrections are negligibly small. The results have been corrected for the tares of the spreader bar and balance housing. The lift and moment corrections were considered negligible. A drag tare which varied from $C_D \approx 0.005$ at low angles of attack to $C_D \approx 0.015$ (when based on 12.27 sq ft area) at high angles of attack was subtracted from the data.

RESULTS AND DISCUSSION

Experimental Results

Effect of twist and camber.- The effect of twist and camber on the longitudinal aerodynamic characteristics are presented in figure 4 for the aspect-ratio-3 parawing and in figure 5 for the aspect-ratio-6 parawing. For the aspect-ratio-3 parawing the results (fig. 4) indicate a maximum lift-drag ratio of about 6.2 for the cambered and twisted parawing (conical-type canopy); this value

is approximately the same as that reported for similar parawing tests. Eliminating the camber and twist by use of cylindrical canopy resulted in a large increase in maximum lift-drag ratio from 6.2 to 10. Similar results were obtained with the aspect-ratio-6 paraglider (fig. 5), the maximum lift-drag ratio increasing from about 7.9 for the conical-type canopy to about 13.6 for the cylindrical-type canopy.

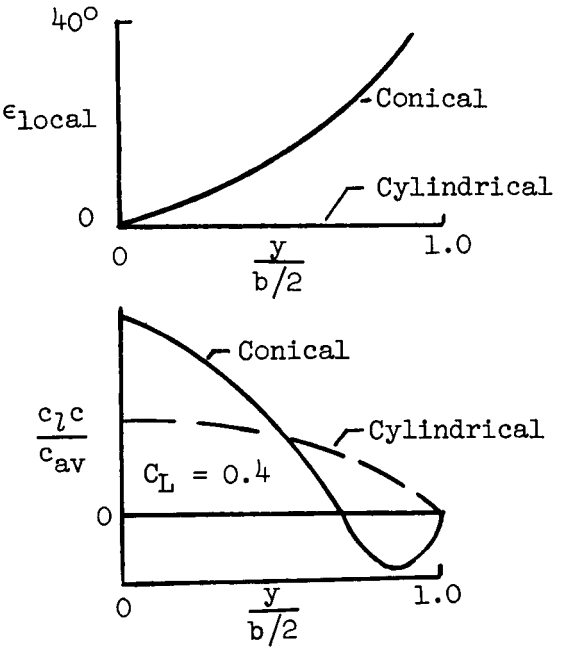

Sketch (a)

The large improvements in the aerodynamic efficiency for the cylindrical canopies can be explained, at least in part, with the aid of sketch (a) where the washout and span-load distributions determined by the methods described in the section "Comparison With Theory" are shown for the two types of canopies. A lift coefficient of 0.4 was selected as representative of the range in which maximum efficiency should occur. For the more conventional conical-type canopy it will be noted that rather extreme washout exists and at moderate lift coefficients this washout may result in a span-load distribution having negative lift loops near the wing tips and, as a result, high induced drag. It would therefore appear that the extreme washout is primarily responsible for the relative low lift-drag ratios for the conical-type canopies. The cylindrical canopies were designed to have zero washout and it can be seen in sketch (a) that the resulting span loading is more nearly elliptical; thereby considerable reduction in induced drag and corresponding increases in maximum lift-drag ratio relative to the more conventional conical canopy parawings are provided.

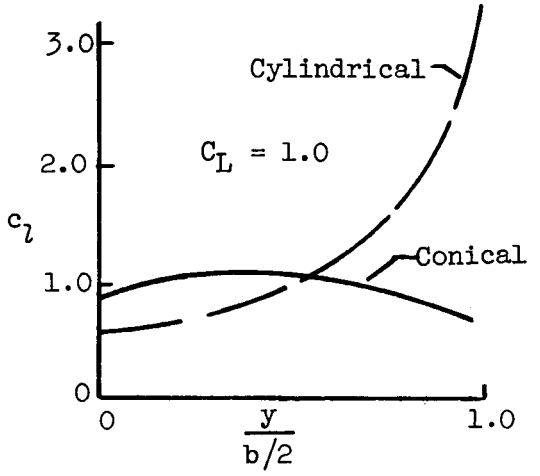

Sketch (b)

Although the cylindrical canopies provided large increases in the maximum lift-drag ratio, they caused losses in lift-drag ratio for lift coefficients above about 0.80 for both the aspect-ratio-3 (fig. 4) and the aspect-ratio-6 (fig. 5) parawings. This result probably was due to the fact that at the higher lift coefficients the spanwise variation of section lift coefficient c_l results in tip stall. This effect is illustrated in sketch (b) where the theoretical

spanwise distribution of the section lift coefficient is presented for both the conical and cylindrical canopies at a wing lift coefficient of 1.0. From sketch (b) it is apparent that the conical-type canopy provides, because of its washout, section lift coefficients that are relatively constant across the span whereas for the cylindrical canopy the section lift coefficient increases rather rapidly near the tip with theoretical lift coefficients that would be expected to be beyond the maximum attainable occurring near the tip. Tip stall and the corresponding high drag would therefore be expected for the cylindrical canopy at high-lift coefficients.

With regard to the effect of camber and twist on the performance of parawings, it appears that, if high aerodynamic efficiency is required, a cylindrical canopy or a slight deviation to provide optimum twist is desirable whereas, if the attainment of high lift is more important than the level of efficiency, a conical canopy may be more desirable.

The effect of twist and camber on the lift characteristics is also shown in figures 4 and 5 and, as would be expected from rigid wing theory, the main effects of reducing the twist and camber by use of the cylindrical canopy are essentially to eliminate the large effective angle for zero lift $\alpha_{L=0}$, to reduce slightly the maximum lift coefficient, and to allow the canopies to load up at keel angles very close to zero. With regard to $\alpha_{L=0}$ it should be pointed out that, since data near zero lift could not be obtained for the conical canopies and would not have corresponded to canopy shapes encountered in the usable lift range, the angle for zero lift is considered as that value obtained by extrapolation of the linear portion of the plots of C_L against α. The fact that the cylindrical canopies load up at keel angles close to zero should be an advantage since it provides a useful range of low lift coefficients not available with the conical canopies.

With regard to the pitching-moment characteristics the largest effect of twist and camber occurred on the aspect-ratio-6.0 paraglider. (See fig. 5.) The largest effect is a change in the "effective" C_{m_o} of about 0.07 (where C_{m_o} is determined by the same technique as $\alpha_{L=0}$). The relative effect of twist and camber will be discussed in the section entitled "Comparison With Theory." The primary reason for the larger effect on the high-aspect-ratio wing is the higher sweep angle of the quarter-chord line which results in a larger relative fore-and-aft displacement between the centers of pressure of the angle-of-attack and twist loadings. As pointed out in reference 10, C_{m_o} has an important effect with regard to the stick force gradients for aircraft-type applications of parawings and a positive value is, of course, desirable. The present results indicate that from this standpoint, the high-aspect-ratio conical canopy would be desirable. The section entitled "Comparison With Theory" presents methods by which it appears that C_{m_o} can be estimated with sufficient accuracy for preliminary design.

Another effect of camber and twist is to delay the unstable break in the pitching moment of the aspect-ratio-6 parawing to higher lift coefficients. The relatively small effect on the aspect-ratio-3 parawing (fig. 4) is due to a smaller degree of twist and the reduction in the sweep of the quarter-chord line.

The change in stability indicated between the conical and cylindrical canopies is due to the difference in reference points. (See fig. 3.)

From the values of C_{m_o} and $\alpha_{L=0}$ it appear that, at least for the lower lift range, the cylindrical-type canopy actually assumed a shape that resulted in some washin. This result might be expected from the fact that the higher load near the root would tend to shift the canopy inboard and thereby lift the trailing edge above the leading edge inboard and result in the trailing edge being below the leading edge over the outboard portion of the canopy.

Effect of tip modification.- In an attempt to improve further the aerodynamic characteristics of the aspect-ratio-6 cylindrical canopy configuration, a finite chord tip was added (fig. 3(d)) in order to reduce the spanwise variation of section lift coefficient. This modification changed the taper ratio from 0 to 0.08. The effects of this modification on the aerodynamic characteristics are presented in figure 6. The primary effect is seen to be an increase in lift-drag ratio over the entire lift-coefficient range, the maximum lift-drag ratio increasing from about 13.6 to about 16.2. Other changes associated with the tip modification are a delay in the occurrence of an unstable break in the pitching moment and a slight increase in the maximum lift coefficient.

Effect of aspect ratio.- The effects of aspect ratio for either the conical or cylindrical canopies can be seen by comparison of figures 4 and 5. Figure 7, however, compares directly the effect of aspect ratio on the cylindrical canopies. These results indicate the usual aspect-ratio effects: a reduction in drag due to lift, an increase in lift-drag ratio, an increase in lift-curve slope, and a pitch-up tendency with an increase in aspect ratio.

The effect of aspect ratio on the lift-drag ratio, which in this investigation was considered to be the primary factor, is presented in figure 8 for both the conical and cylindrical canopies. These results indicate rather sizable improvements in lift-drag ratio above a lift coefficient of about 0.4 as the aspect ratio was increased from 3 to 6 for both the conical and the cylindrical canopies.

The models tested had spreader bars in order to provide a constant planform throughout the angle-of-attack range. The structural weight required to assure that sufficient wing span is maintained either through spreader bars or leading edge and apex stiffness for any particular application can be determined only after pertinent aerodynamic load characteristics are known. To maintain the same wing loading, the aspect-ratio-6 parawing requires approximately 45 percent greater span than the aspect-ratio-3 parawing, and an increase in structural weight might be expected. It should be kept in mind, however, that for the same leading-edge sweep angle the aerodynamic load is shifted toward the apex as the aspect ratio is increased; this shifting tends to reduce the leading-edge closing moments for a given span and lift. A simplified analysis indicates that this reduction may be of sufficient magnitude to offset the effect of the required increased span; however, the increase in leading-edge compression must also be considered. Detailed wind-tunnel studies of the aerodynamic loads and free glide tests are needed to clarify the structural aspects.

As mentioned in the previous section the high-aspect-ratio conical parawing provides for a rather large positive value of C_{m_0} which could be further increased if desired by use of a "fuller" canopy which provides a greater degree of washout. Although this type of canopy would probably reduce the maximum lift-drag ratios, the possible improvements in trim and stick force gradients when viewed in light of the relatively high lift-drag ratios afforded by the high aspect ratio may make the fuller canopy desirable for some applications. For the lower aspect ratio conical parawing the effect of the washout is reduced such that the camber effect predominates and a negative value of C_{m_0} results (see fig. 4).

Comparison With Theory

Procedures used in estimates.- In order to make theoretical estimates of the aerodynamic characteristics of the various parawings tested, it was necessary to estimate the camber and twist distribution. For the cylindrical-type canopies, it was assumed that in the fully loaded condition the canopy had negligible camber and twist. For the conical-type canopies it was assumed that in the fully loaded condition each semispan assumed a shape approximating a portion of a cone and the camber and twist for several spanwise stations parallel to the plane of symmetry were determined by the method described in the appendix. The nondimensional camber lines for several spanwise stations are compared in the upper part of figure 9 for both the aspect-ratio-6 and aspect-ratio-3 conical parawings. The chord lines have been made coincident to facilitate comparison of the camber distributions; the chord-line twist distributions are also presented in figure 9. With regard to the camber lines it is interesting to note that the camber increases from zero at the root (or keel) to nearly 5 percent at the 20-percent semispan station and then decreases to zero at the tip. Inboard, the camber is relatively far forward whereas near the tip it is essentially a circular arc. The geometric twist distribution indicates rather extreme values, approximately 34° occurring for both aspect ratios.

The zero-lift line for each camber line was determined by the Pankhurst method (ref. 11) and the spanwise variations are presented in the top part of figure 10. The aerodynamic twist was then determined from the difference between the zero-lift lines and the geometric twist (fig. 9) and is presented in figure 10.

The effect of camber on the zero-lift pitching moment was also determined by the method of reference 11 (reduced by $\cos \Lambda$ to approximate sweep effects) and the effect of twist on the angle for zero lift and zero-lift pitching moment was determined from the Weissinger 15-point modified lifting-line span loadings presented in references 12 and 13. The $\alpha_{L=0}$ due to camber is presented in figure 10. The aerodynamic twist distributions were approximated by combinations of linear and quadratic distributions of twist, for which analytic solutions are available in references 12 and 13, as shown in figure 10. For the aspect-ratio-6 conical parawing, a 40° linear washout combined with 6° quadratic washin (40° linear - 6° quadratic) results in a good approximation to the actual twist distribution. (Compare solid line values with square symbol values in fig. 10.) For the aspect-ratio-3 parawing, a 10° linear washout combined with 25° quadratic washout (10° linear + 25° quadratic) provides sufficient accuracy. The angles for zero lift and zero-lift pitching moments due to the actual twist were then

estimated by combining the theoretical values for the various combinations of linear and quadratic twist distributions.

For convenience in making similar estimates for other configurations, calculations for linear, quadratic, and cubic twist distributions were made for a range of planforms and are presented in figure 11. The twist distributions are defined as follows:

linear:

$$\epsilon_{local} = \epsilon\left(\frac{y}{b/2}\right)$$

quadratic:

$$\epsilon_{local} = \epsilon\left(\frac{y}{b/2}\right)^2$$

and cubic:

$$\epsilon_{local} = \epsilon\left(\frac{y}{b/2}\right)^3$$

It should be noted that the results presented in figure 11 are for a unit value of ϵ. All theoretical calculations, when applied to the parawings, were based on the projected planforms and the resulting coefficients converted to the flat canopy reference area and chord.

Lift characteristics.- With regard to the lift characteristics, estimates were made of the angle for zero lift $\alpha_{L=0}$ and the lift-curve slope. No attempt to estimate the maximum lift was made. The Weissinger modified lifting-line method was used and the characteristics were computed for the projected planform and converted to the reference areas. The two-dimensional lift-curve slope required in the theory has not been established for the type of airfoil sections involved; however, tests of the Farman airfoil (ref. 14), which is somewhat similar, indicates a value of c_{l_α} of about 0.09 per degree and this value was used in the calculations. The aerodynamic twist distribution was approximated for the aspect-ratio-6 parawing by subtracting a 6° quadratic twist distribution from a 40° linear twist distribution as described previously. The angle of zero lift for the 40° linear twist (13.7°) obtained from figure 11 was reduced by the angle of zero lift (1.1°) for the 6° quadratic twist also obtained from figure 11 to give a final value of 12.6°. This angle for zero lift when combined with the theoretical lift-curve slope results in reasonably good agreement between the estimated and measured lift characteristics for the aspect-ratio-6 conical parawing as shown in figure 12(b). The lift-curve slope agreement appears to be within the experimental accuracy and, although the theoretical angle for zero lift is displaced in the positive direction for both canopies, the theory appears to predict fairly accurately the difference between the two canopies. The shift in the angle for zero lift between the experiment and theory is believed to be associated primarily with an inboard shift in the canopy relative to the assumed conical and cylindrical shapes that reduces the washout. This type of shift

would be expected from the distribution of load and has been observed in photographs of paragliders under test.

Pitching-moment characteristics.- A comparison of the estimated and measured pitching-moment characteristics is presented in figure 13. The value of the pitching-moment coefficient at zero lift C_{m_o} for the parawings having conical-type canopies was estimated by combining the theoretical effect due to the aerodynamic twist distribution (fig. 10) as determined from figure 11 with that due to camber as determined by the Pankhurst method (ref. 11). The effect of twist was, of course, determined for the same combination of linear and quadratic twist as described in the previous section. The slope of the pitching-moment curve was also determined by the Weissinger method from which the following approximation for the distance from the leading edge of the root chord to the aerodynamic center in fraction of root chord length can be obtained for $\lambda = 0$.

$$\frac{x_{ac}}{c_k} = 0.25\left(1 + 0.4A \tan \Lambda_{c/4}\right)$$

The resulting pitching-moment estimates for the conical-type paragliders are in reasonably good agreement with experiment and indicate that the method used should be of sufficient accuracy for preliminary design requirements.

For the cylindrical canopies a value of C_{m_o} of zero would be expected; however, as discussed in the section on lift some effective washin appears to exist that results in a negative value of C_{m_o}. In an attempt to correlate this negative value of C_{m_o} with the negative value of $\alpha_{L=0}$ indicated in figure 12 the theoretical C_{m_o} due to a linear washin of magnitude sufficient to produce the measured $\alpha_{L=0}$ was determined from figure 11 for the two cylindrical-type parawings. The measured value of $\alpha_{L=0}$ was defined as that obtained by shifting the theoretical lift-curve slope until it was tangent to the experimental curve at $C_L = 0.40$. The resulting estimated pitching-moment curves are seen to be in good agreement with experiment for the aspect-ratio-6 cylindrical parawing, in the moderate lift-coefficient range. However, for the $A = 3$ cylindrical parawing, the agreement is rather poor. The effect of canopy shape on the stability level $\frac{\partial C_m}{\partial C_L}$ is due to the difference in moment reference points. (See fig. 3.)

CONCLUSIONS

Based on low-speed wind-tunnel tests of a series of parawings having conical- and cylindrical-type canopies, the following conclusions were reached:

1. Parawings having cylindrical canopies (essentially zero camber and twist) provide considerably higher maximum lift-drag ratios than the more conventional conical type, an increase from 6.2 to 10 occurring for an aspect-ratio-3 parawing and from 7.9 to 13.6 for an aspect-ratio-6 parawing. However, for lift coefficients above about 0.80, the conical canopies provided higher lift-drag ratios.

2. For a given leading-edge sweep, the largest effect of canopy shape (camber and twist) on the pitching-moment coefficient C_{m_o} occurred for the high-aspect ratio due primarily to the higher quarter-chord sweep, with the aspect-ratio-6 conical type providing a rather large positive value of effective C_{m_o}.

3. Comparison with theory indicated that use of the Pankhurst method for camber effects and use of the Weissinger method for angle-of-attack and twist effects provide sufficient accuracy for preliminary aerodynamic design.

4. The improvements in aerodynamic efficiency and the zero-lift pitching-moment characteristics indicated for the high-aspect-ratio parawing appear to be sufficient to warrant more detailed free-flight investigation.

5. The cylindrical canopies loaded up at low angles of attack; thus a useful range of low lift coefficients not available with the conical surface parawings was provided.

Langley Research Center,
National Aeronautics and Space Administration,
Langley Station, Hampton, Va., October 26, 1962.

APPENDIX

CALCULATIONS OF AIRFOIL PROFILES USED IN APPLICATION OF THEORY

The airfoil profiles at several spanwise stations were determined in the process of applying theory to calculations of the aerodynamic characteristics of the conical parawings. The method of determining the airfoil sections is given here for those interested in extending the calculations to other parawing configurations.

Each wing panel of the parawing was assumed to be a part of the surface of a circular cone as shown in sketch (c).

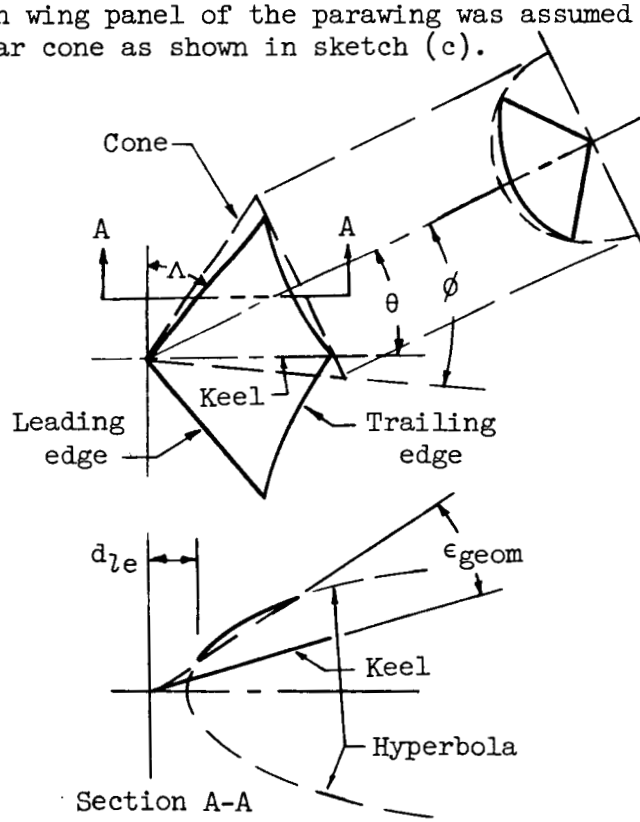

Sketch (c)

The streamwise airfoil sections can be shown (ref. 15, for example) to be parts of the hyperbolas formed by cutting planes parallel to the keel and normal to the line connecting the wing tips. The equation for the hyperbolas is

$$\frac{X^2}{a^2} - \frac{Y^2}{e^2} = 1 \quad \text{where}$$

$$a = \frac{1}{2}\frac{y}{b/2}\cos\Lambda\left[\frac{1}{\tan(\phi + \theta)} + \frac{1}{\tan(\phi - \theta)}\right]$$

and

$$e = \sqrt{a \frac{y}{b/2} \cos \Lambda \tan \phi}$$

The distance to the leading edge of the section is given by:

$$d_{le} = \frac{1}{2} \frac{y}{b/2} \cos \Lambda \left[\frac{1}{\tan(\phi - \theta)} - \frac{1}{\tan(\phi + \theta)} + \frac{2}{\tan 2\theta} \right]$$

The keel length is taken as unity in these equations. The trailing-edge line was located on the planview by transferring points from the flat planform layout. The distance to the trailing edge was measured along the streamwise sections. The graphical method should be sufficiently accurate because the section slopes are low in the trailing-edge region. A typical section obtained is shown in the sketch. A comparison of the camber distribution for various spanwise stations is presented in figure 9 where the section is rotated through the geometric twist angle and nondimensionalized to facilitate comparisons.

REFERENCES

1. Rogallo, Francis M.: Paraglider Recovery Systems. Presented at IAS Meeting on Man's Progress in the Conquest of Space (St. Louis, Mo.), Apr. 30-May 1-2, 1962.

2. Rogallo, Francis M., Lowry, John G., Croom, Delwin R., and Taylor, Robert T.: Preliminary Investigation of a Paraglider. NASA TN D-443, 1960.

3. Taylor, Robert T.: Wind-Tunnel Investigation of Paraglider Models at Supersonic Speeds. NASA TN D-985, 1961.

4. Penland, Jim A.: A Study of the Aerodynamic Characteristics of a Fixed Geometry Paraglider Configuration and Three Canopies With Simulated Variable Canopy Inflation at a Mach Number of 6.6. NASA TN D-1022, 1962.

5. Naeseth, Rodger L.: An Exploratory Study of a Parawing as a High-Lift Device for Aircraft. NASA TN D-629, 1960.

6. Hewes, Donald E.: Free-Flight Investigation of Radio-Controlled Models With Parawings. NASA TN D-927, 1961.

7. Hatch, Howard G., Jr., and McGowan, William A.: An Analytical Investigation of the Loads, Temperatures, and Ranges Obtained During the Recovery of Rocket Boosters by Means of a Parawing. NASA TN D-1003, 1962.

8. Fournier, Paul G., and Bell, B. Ann: Low Subsonic Pressure Distributions on Three Rigid Wings Simulating Paragliders With Varied Canopy Curvature and Leading-Edge Sweep. NASA TN D-983, 1961.

9. Fournier, Paul G., and Bell, B. Ann: Transonic Pressure Distributions on Three Rigid Wings Simulating Paragliders With Varied Canopy Curvature and Leading-Edge Sweep. NASA TN D-1009, 1962.

10. Johnson, Joseph L., Jr.: Low-Speed Wind-Tunnel Investigation To Determine the Flight Characteristics of a Model of a Parawing Utility Vehicle. NASA TN D-1255, 1962.

11. Pankhurst, R. C.: A Method for the Rapid Evaluation of Glauert's Expressions for the Angle of Zero Lift and the Moment at Zero Lift. R. & M. No. 1914, British A.R.C., 1944.

12. Diederich, Franklin W., and Zlotnick, Martin: Calculated Spanwise Lift Distributions, Influence Functions, and Influence Coefficients for Unswept Wings in Subsonic Flow. NACA Rep. 1228, 1955. (Supersedes NACA TN 3014.)

13. Diederich, Franklin W., and Zlotnick, Martin: Calculated Spanwise Lift Distributions and Aerodynamic Influence Coefficients for Swept Wings in Subsonic Flow. NACA TN 3476, 1955.

14. Von Mises, Richard: Theory of Flight. McGraw-Hill Book Co., Inc., 1945.

15. Wilson, W. A., and Tracey, J. I.: Analytic Geometry. Third ed., D. C. Heath and Co., c.1949.

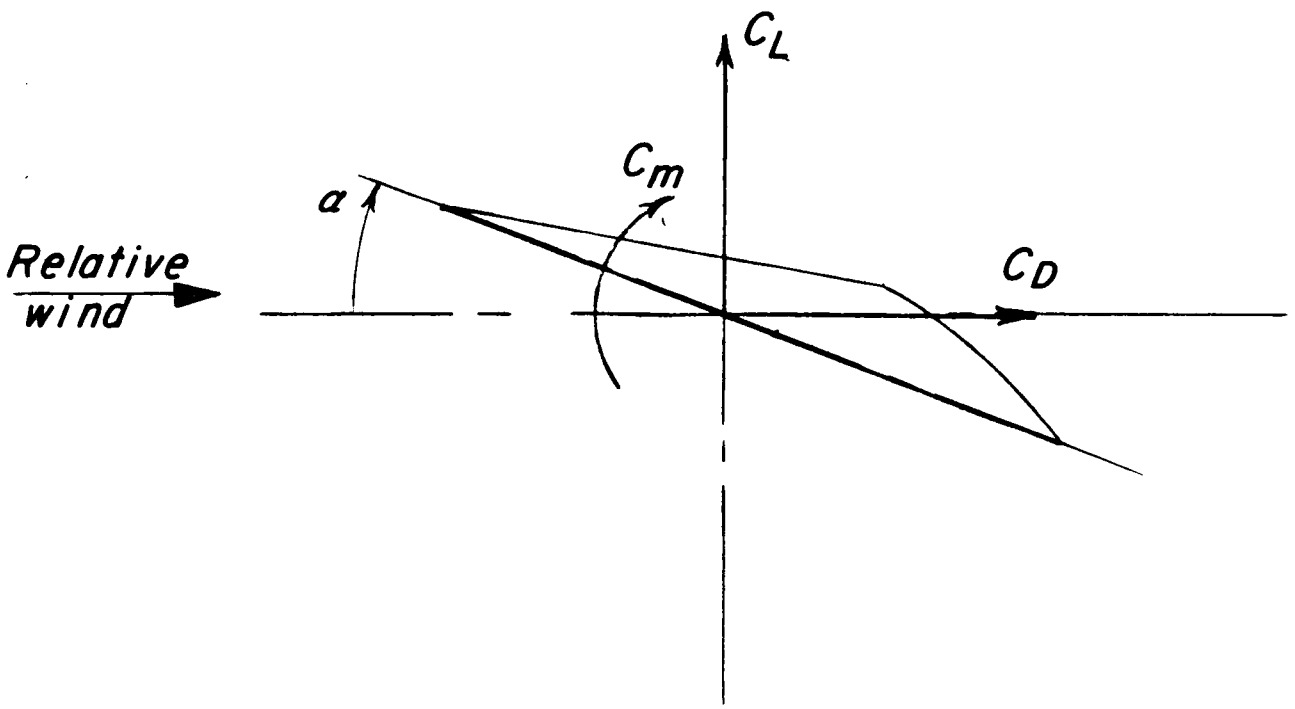

Figure 1.- System of axes. Positive directions are shown by arrows.

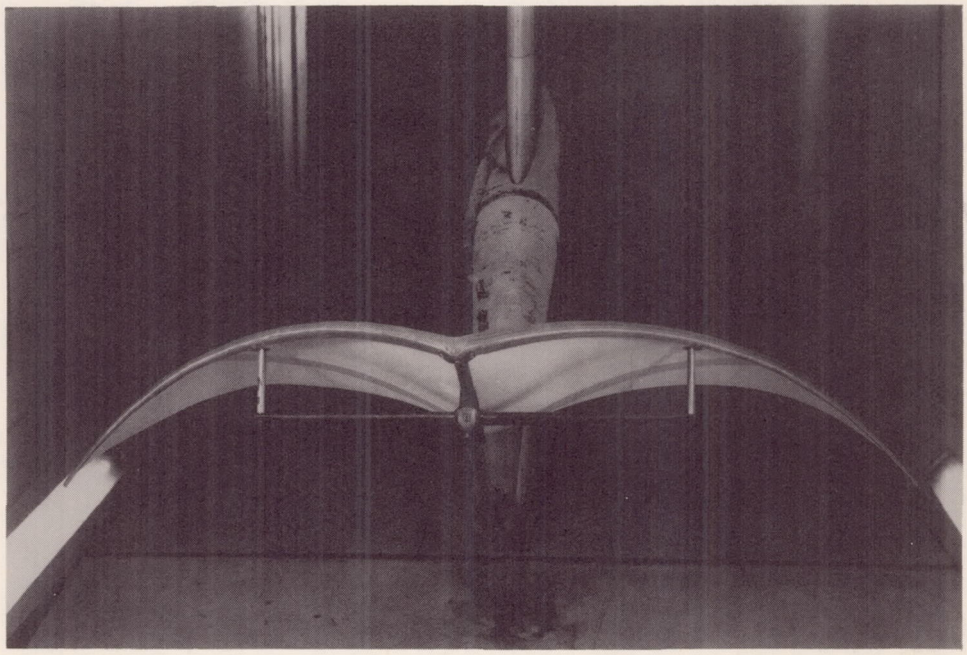

(a) Cylindrical-type canopy. L-62-2940

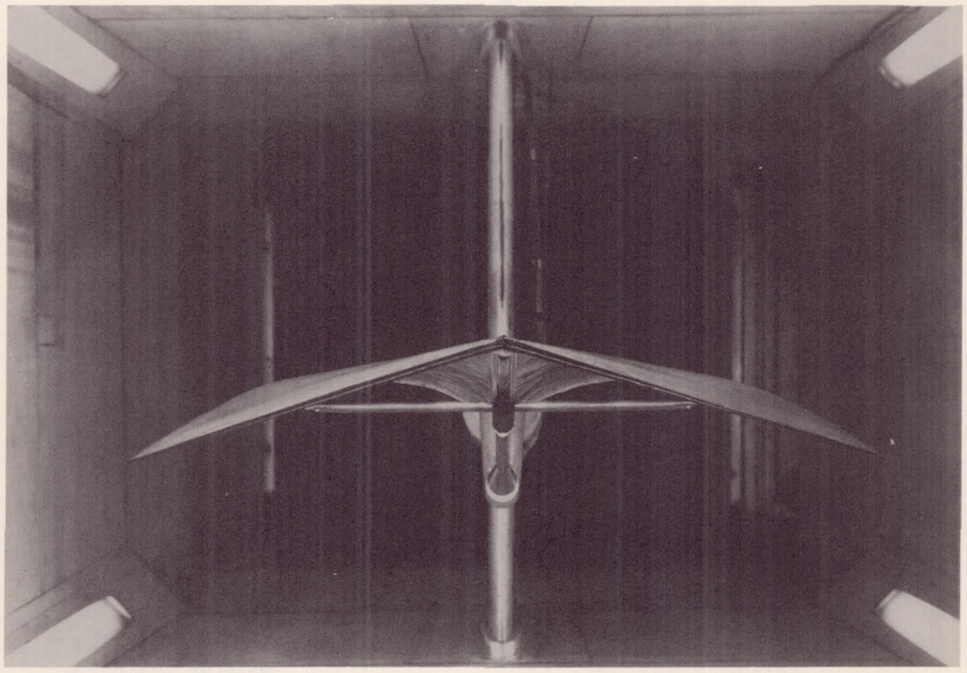

(b) Conical-type canopy. L-62-1686

Figure 2.- High-aspect-ratio models on the sting support system.

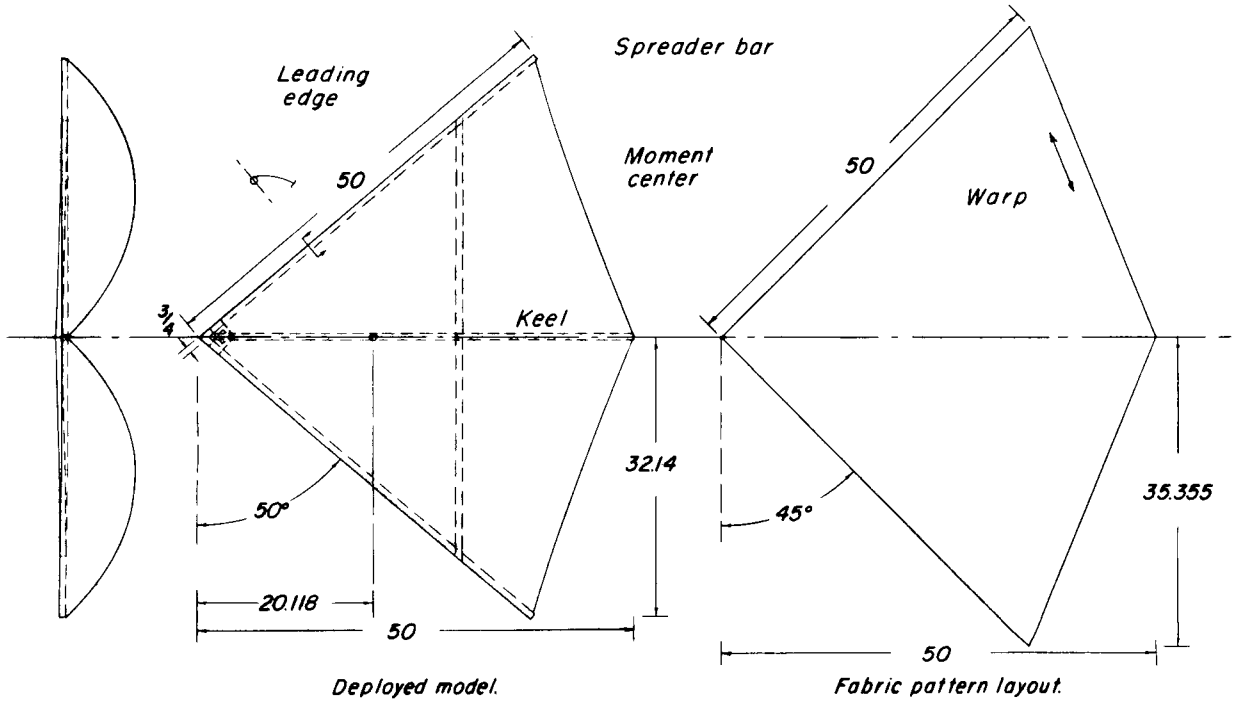

(a) Aspect-ratio-2.8 conical wings.

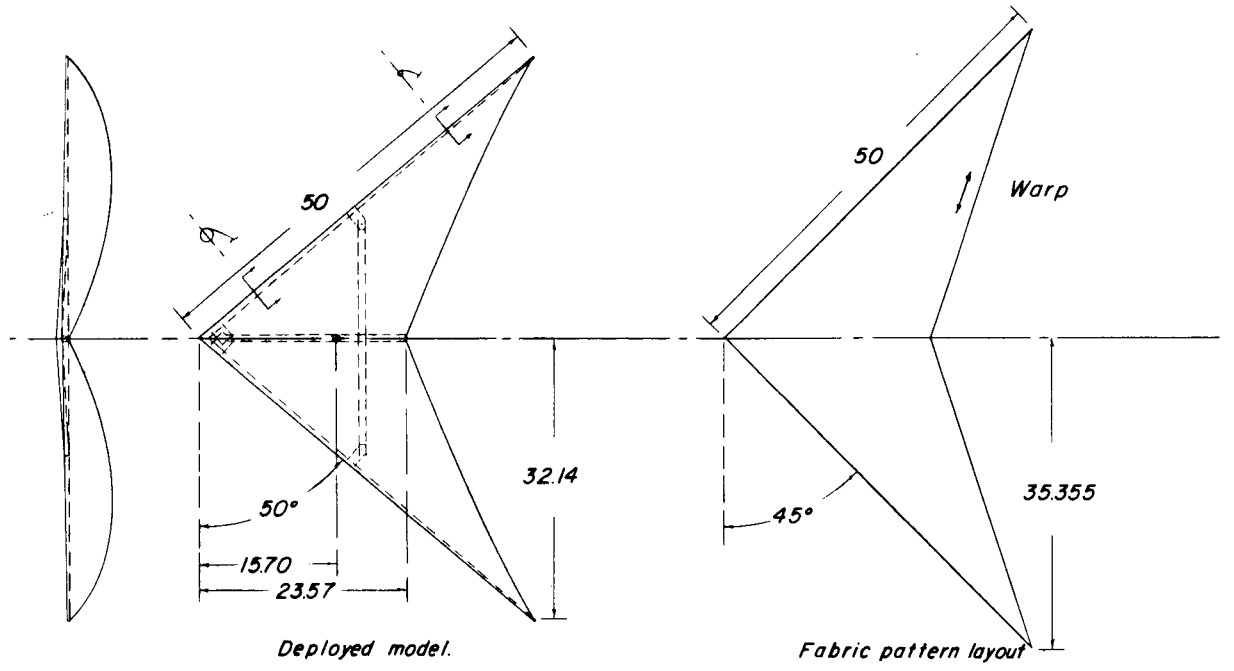

(b) Aspect-ratio-6 conical wings.

Figure 3.- Geometry of models. All dimensions are in inches.

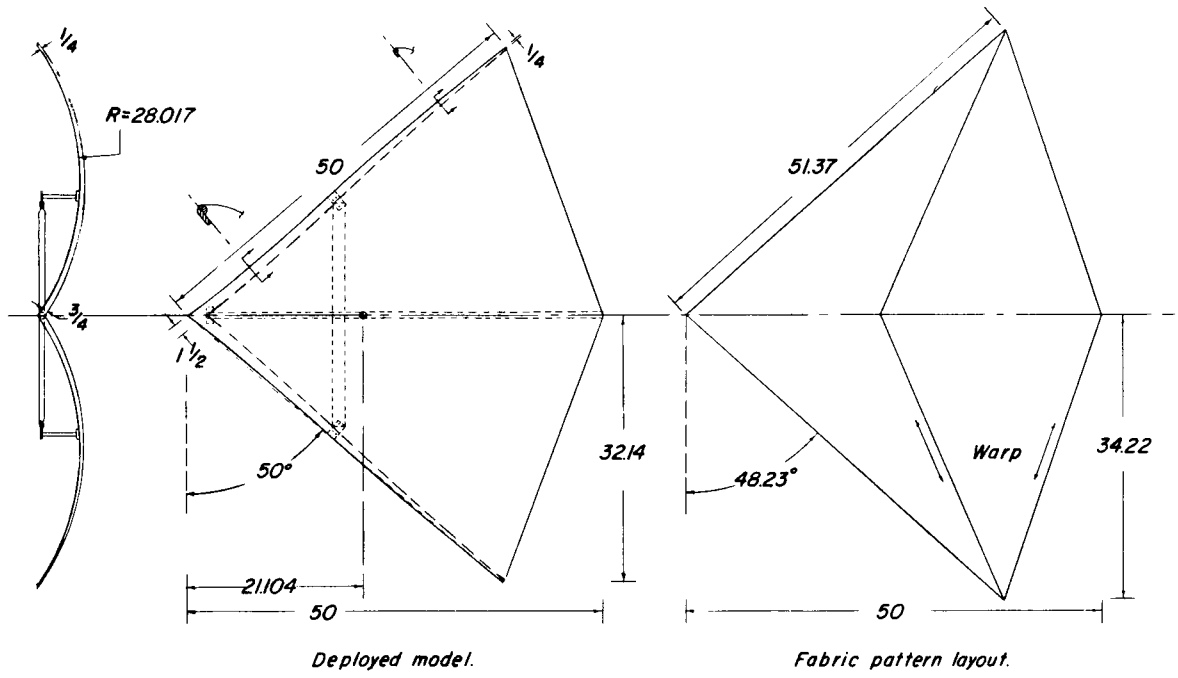

(c) Aspect-ratio-2.7 cylindrical wings.

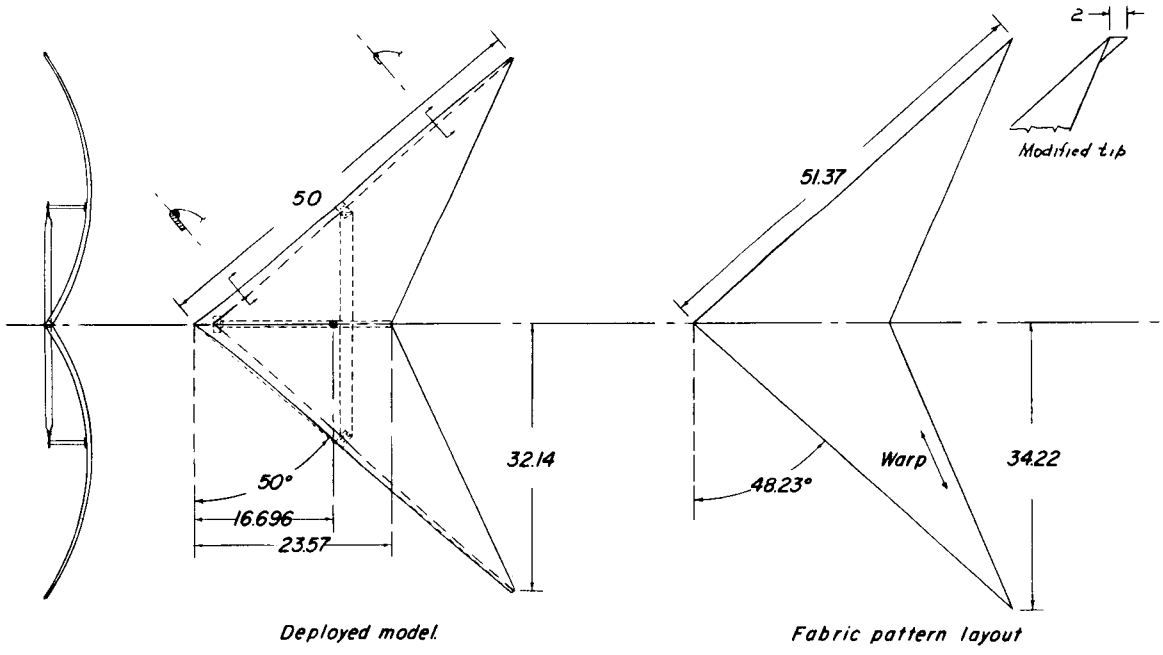

(d) Aspect-ratio-5.8 cylindrical wings.

Figure 3.- Concluded.

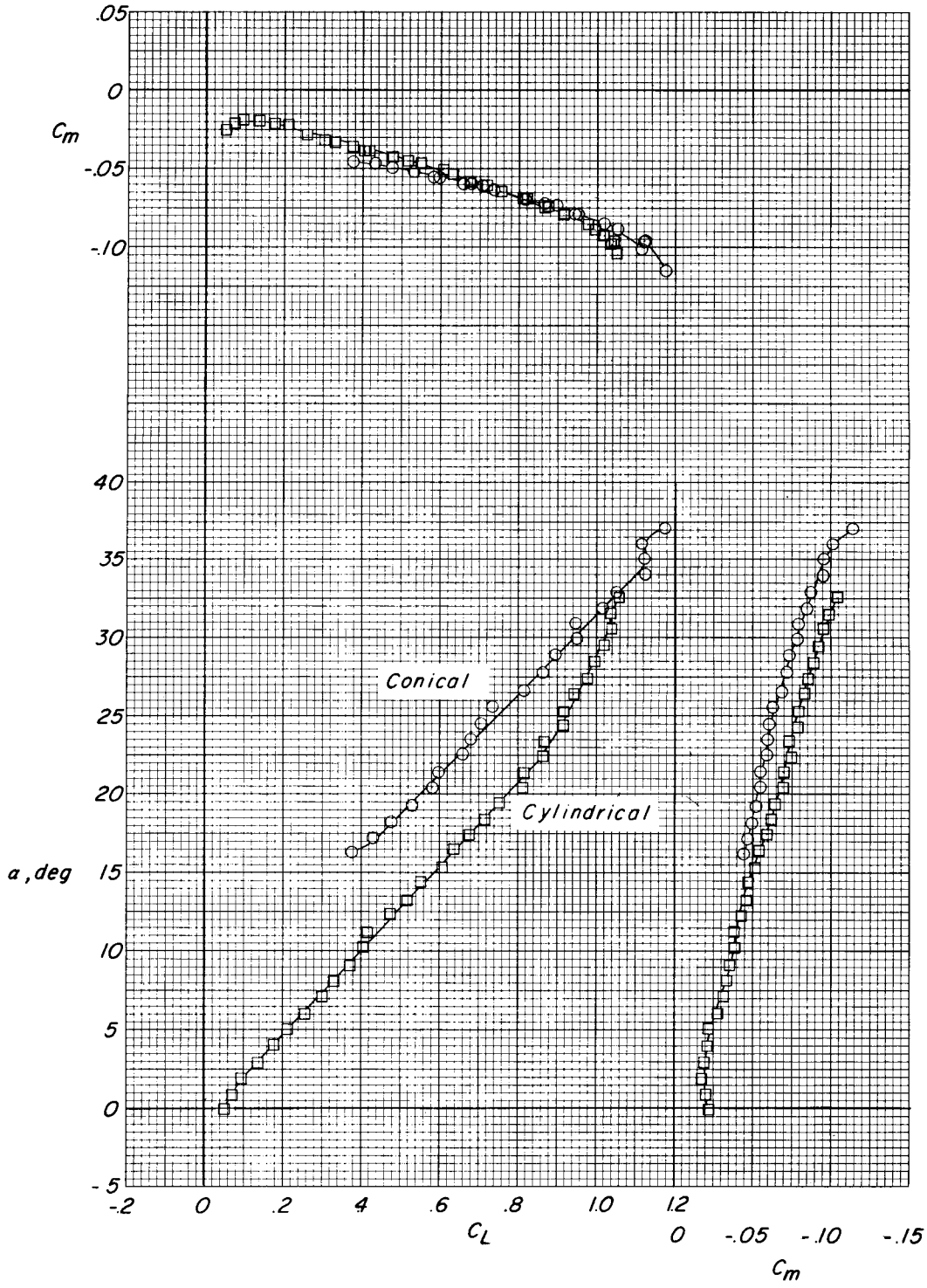

Figure 4.- Comparison of the longitudinal aerodynamic characteristics of paragliders having conical (twisted and cambered) and cylindrical (no twist or camber) surfaces. A = 3.

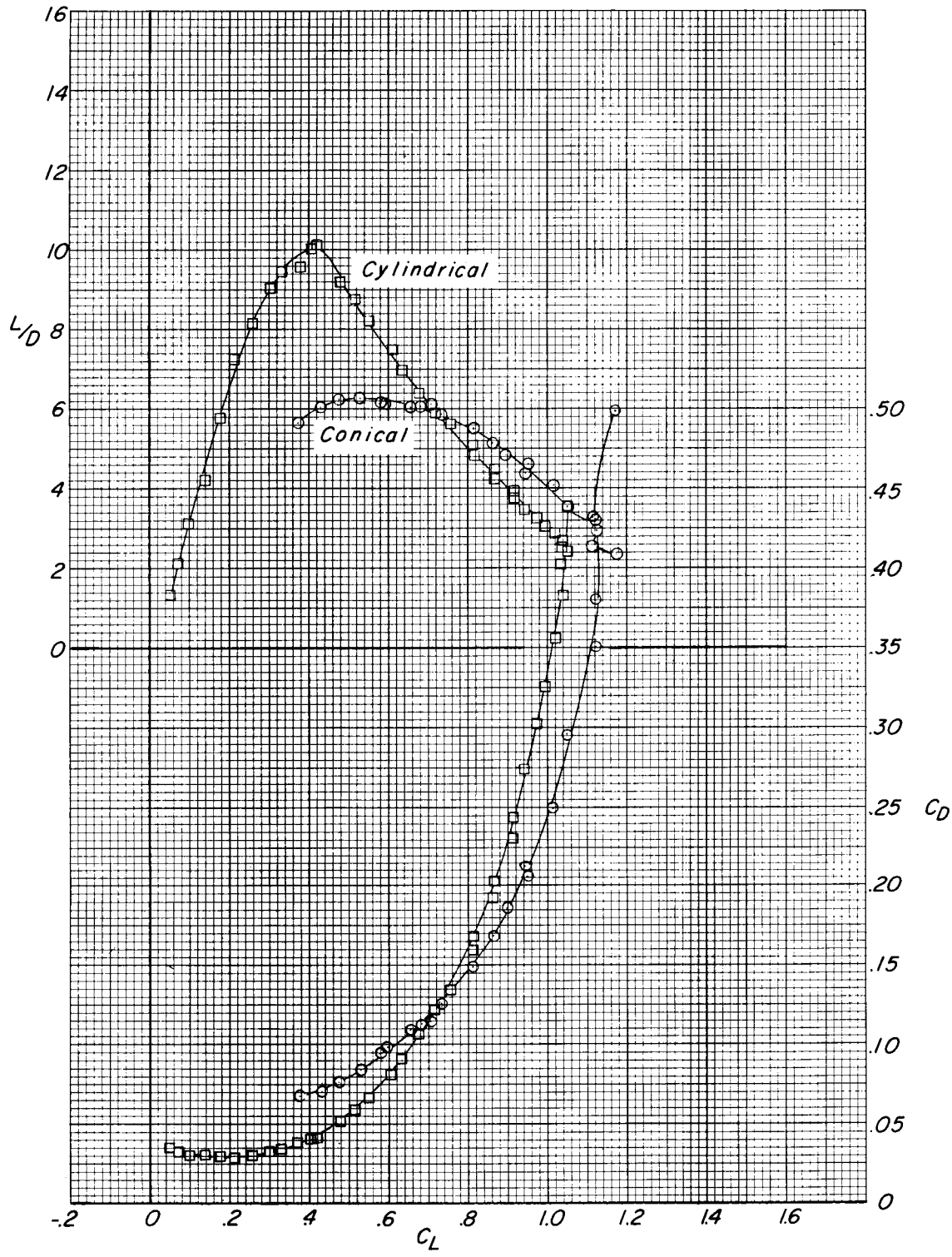

Figure 4.- Concluded.

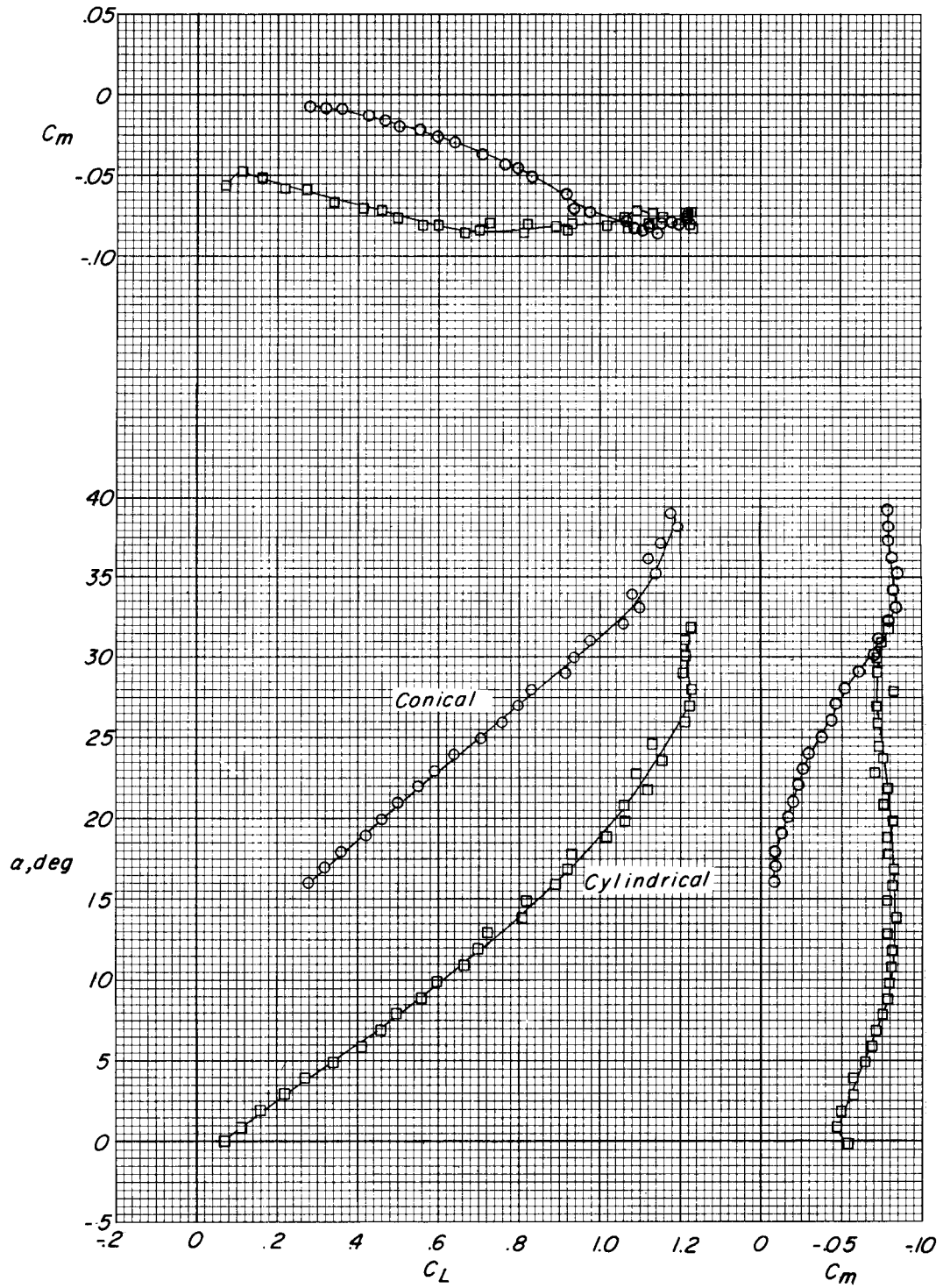

Figure 5.- Comparison of the longitudinal aerodynamic characteristics of paragliders having conical (twisted and cambered) and cylindrical (no twist or camber) surfaces. A = 6.

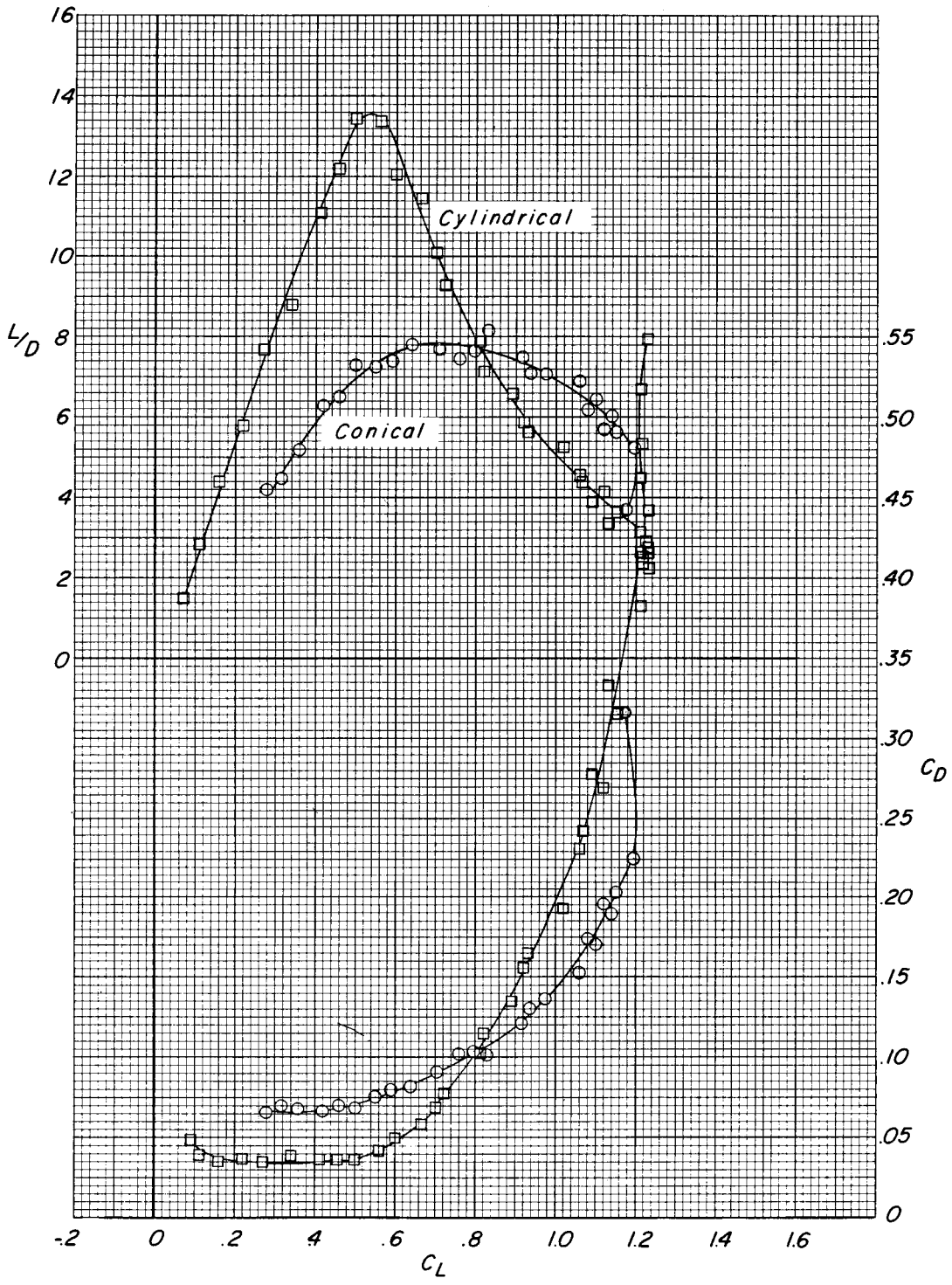

Figure 5.- Concluded.

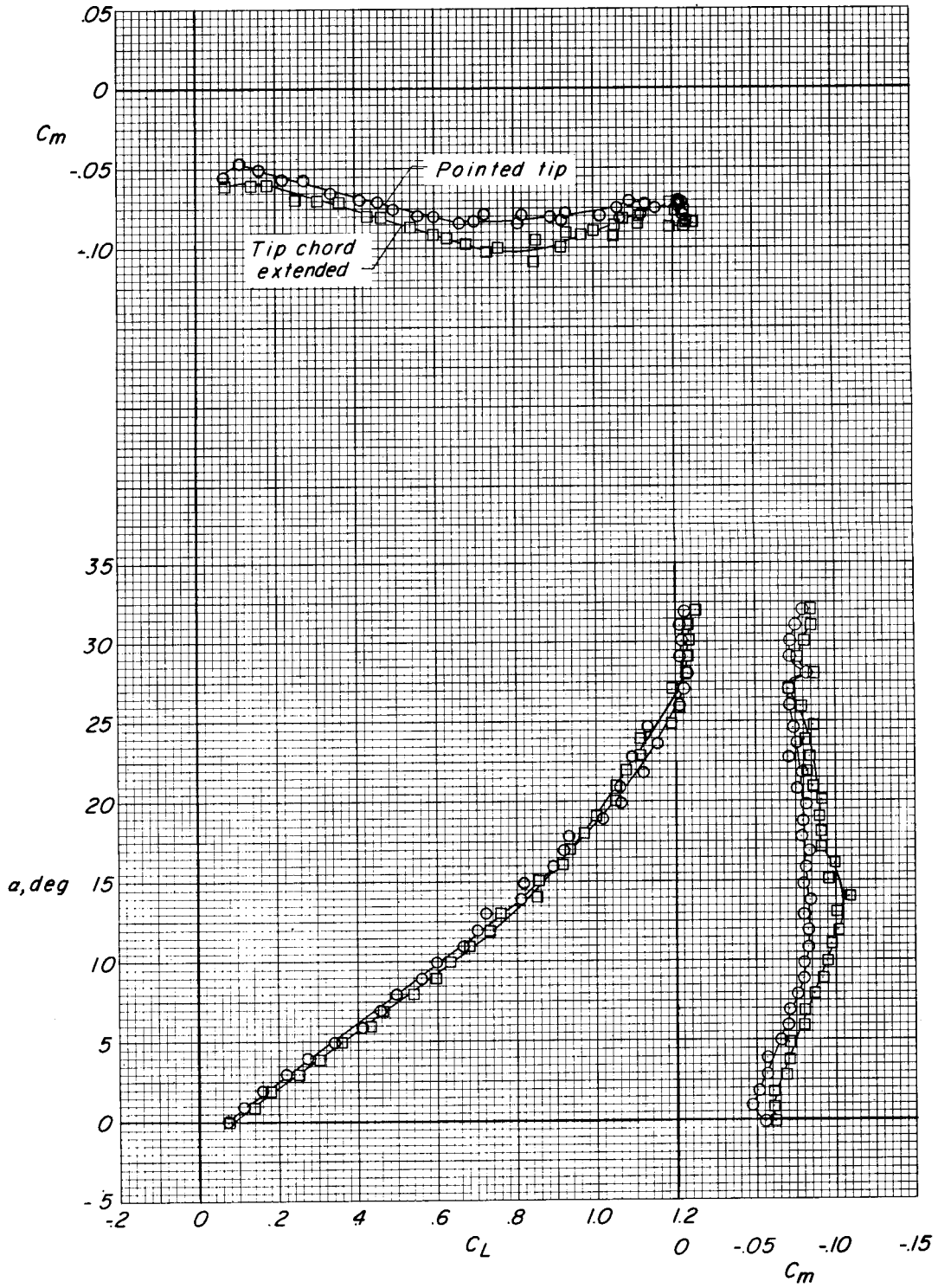

Figure 6.- Effect of tip modification on the longitudinal aerodynamic characteristics of a paraglider having a cylindrical surface. A = 6.

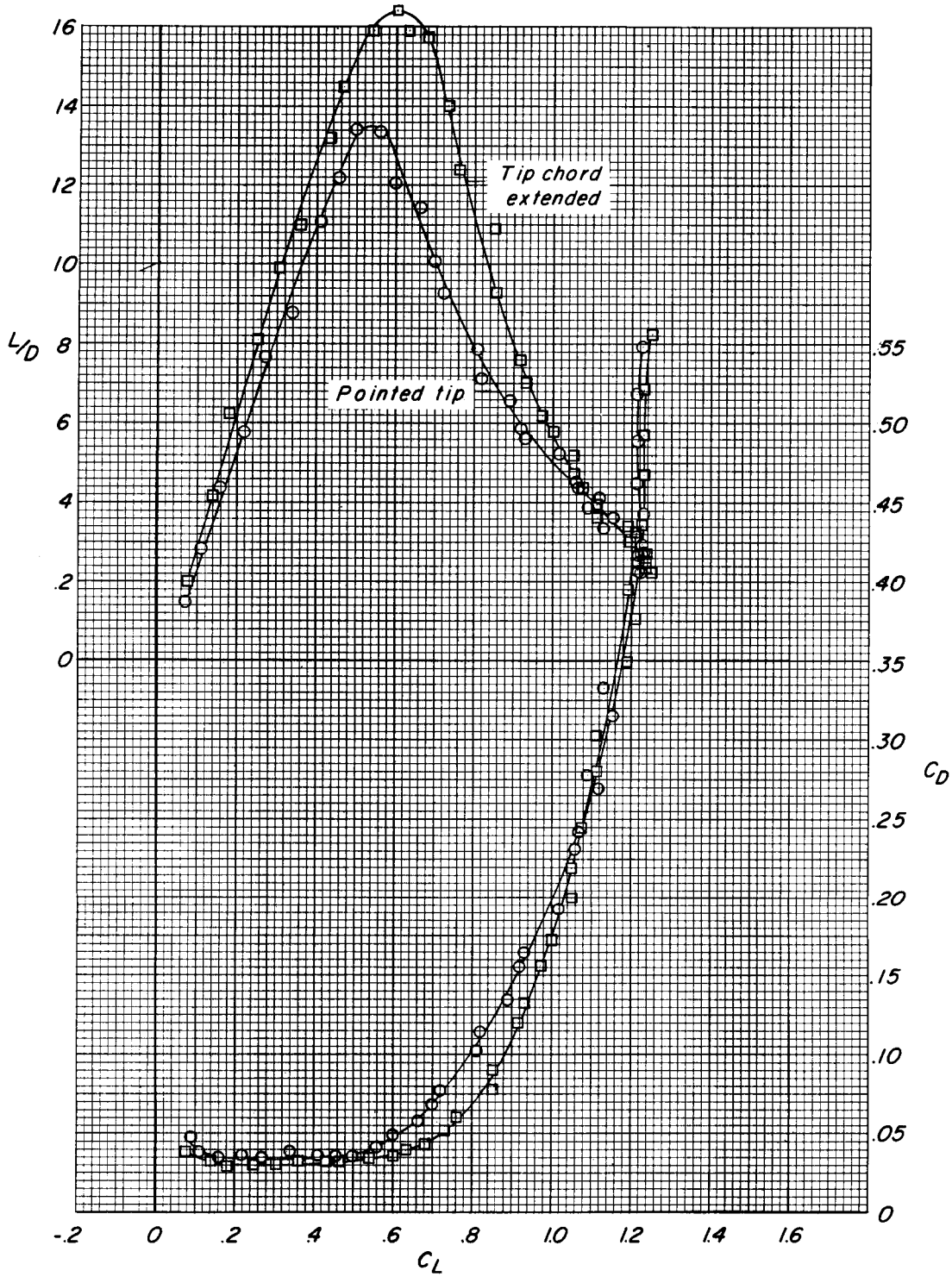

Figure 6.- Concluded.

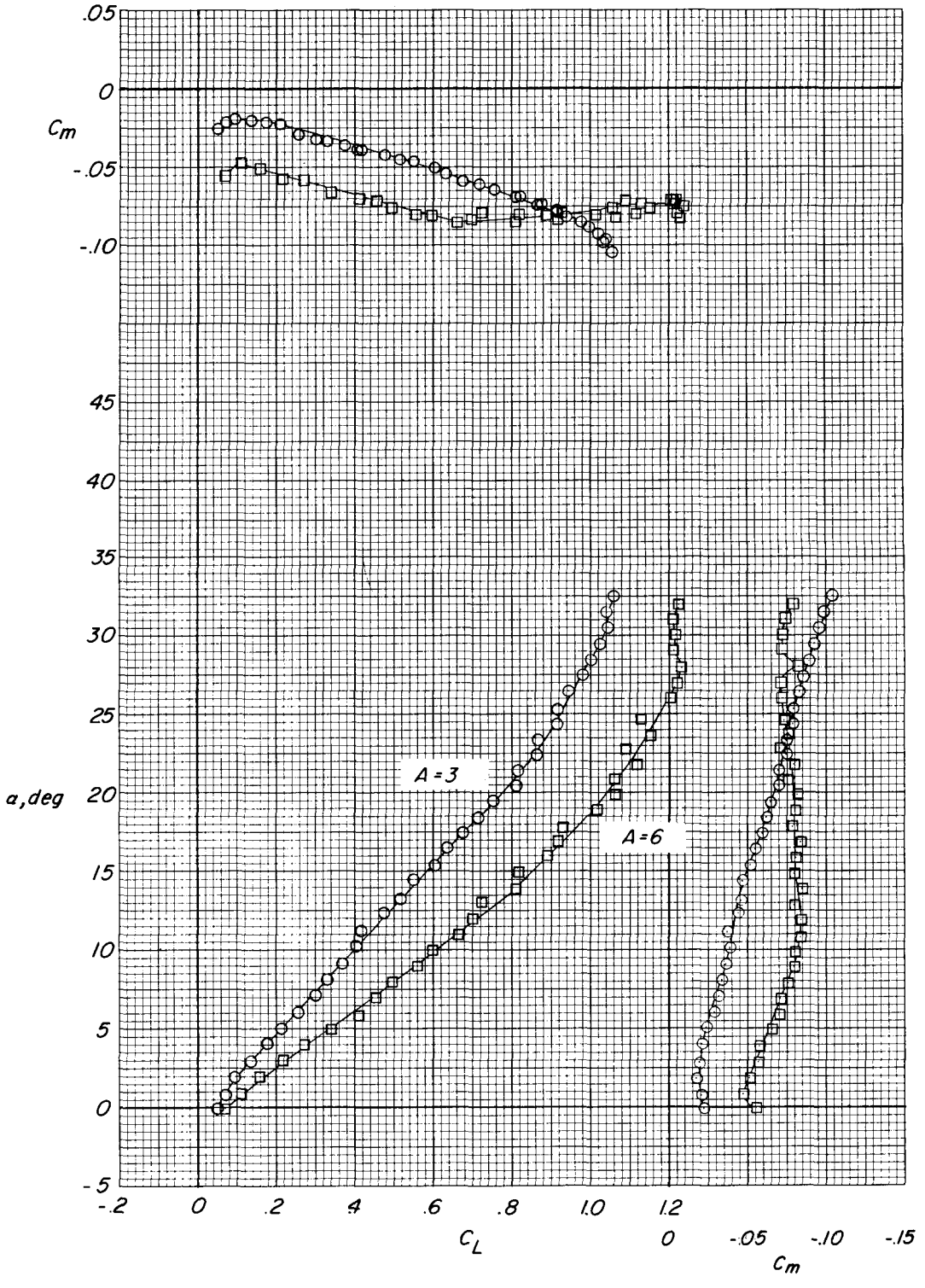

Figure 7.- Effect of aspect ratio on the longitudinal aerodynamic characteristics of paragliders having cylindrical surfaces.

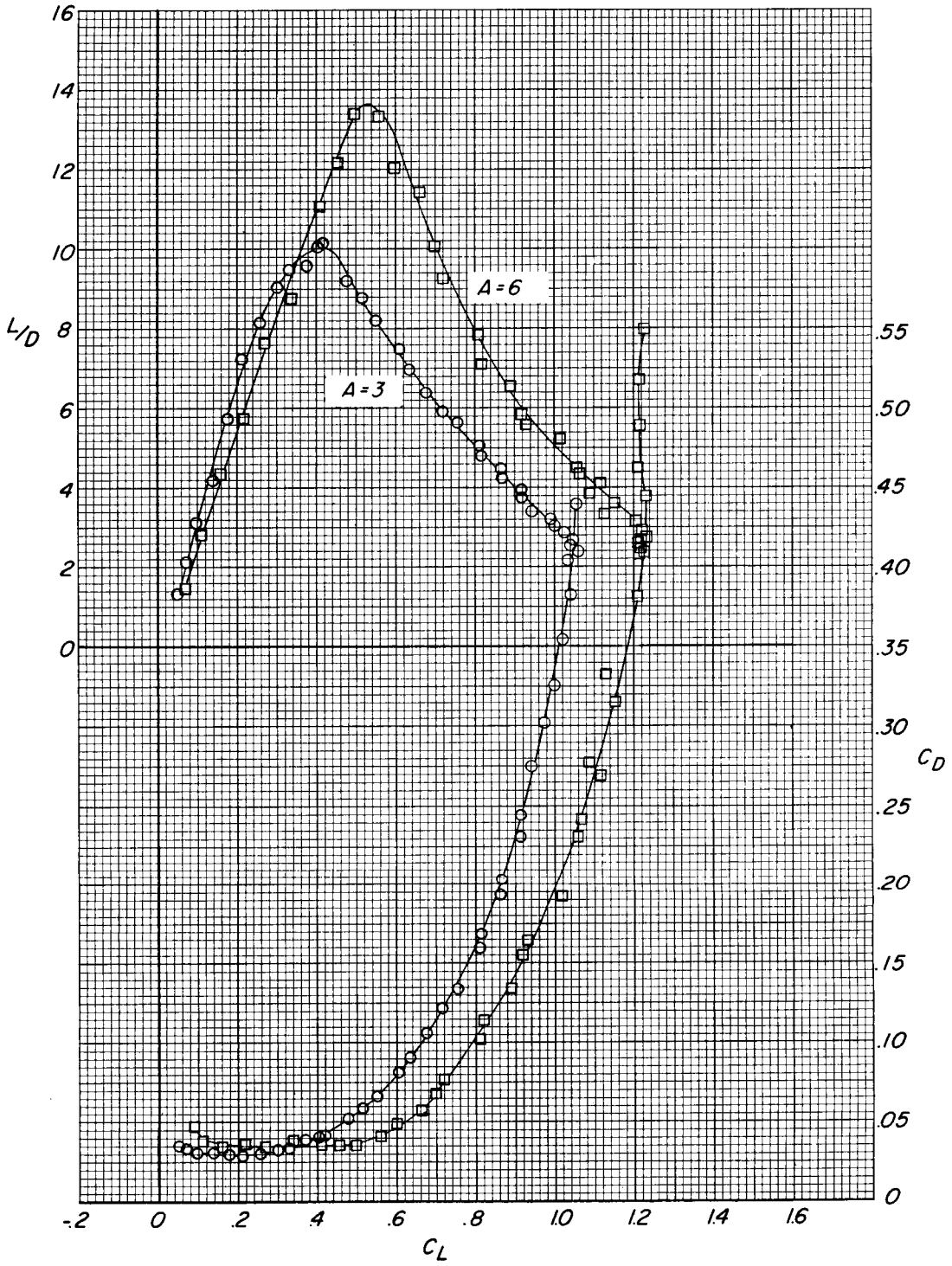

Figure 7.- Concluded.

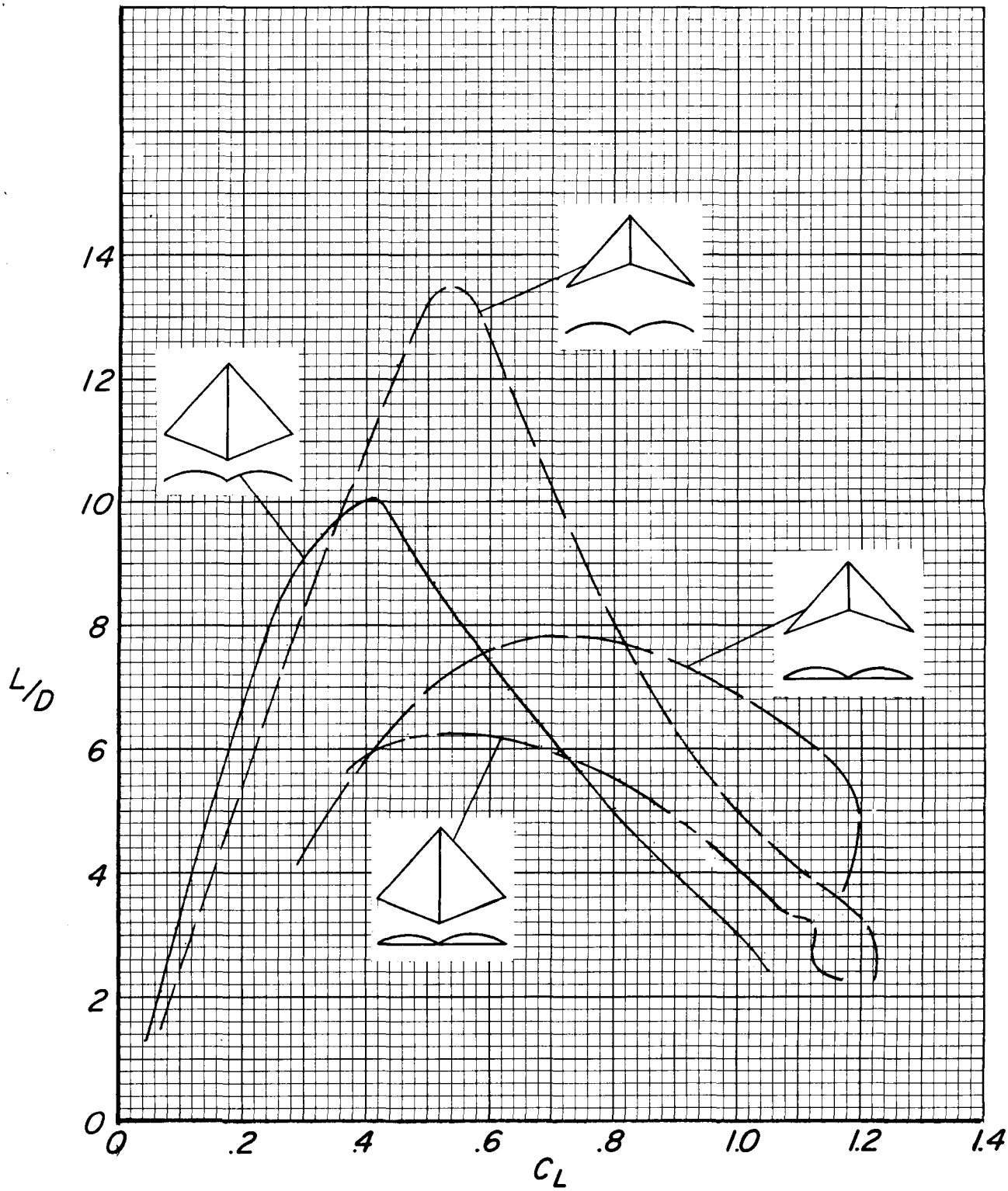

Figure 8.- Lift-drag ratios for parawings with conical and cylindrical surfaces.

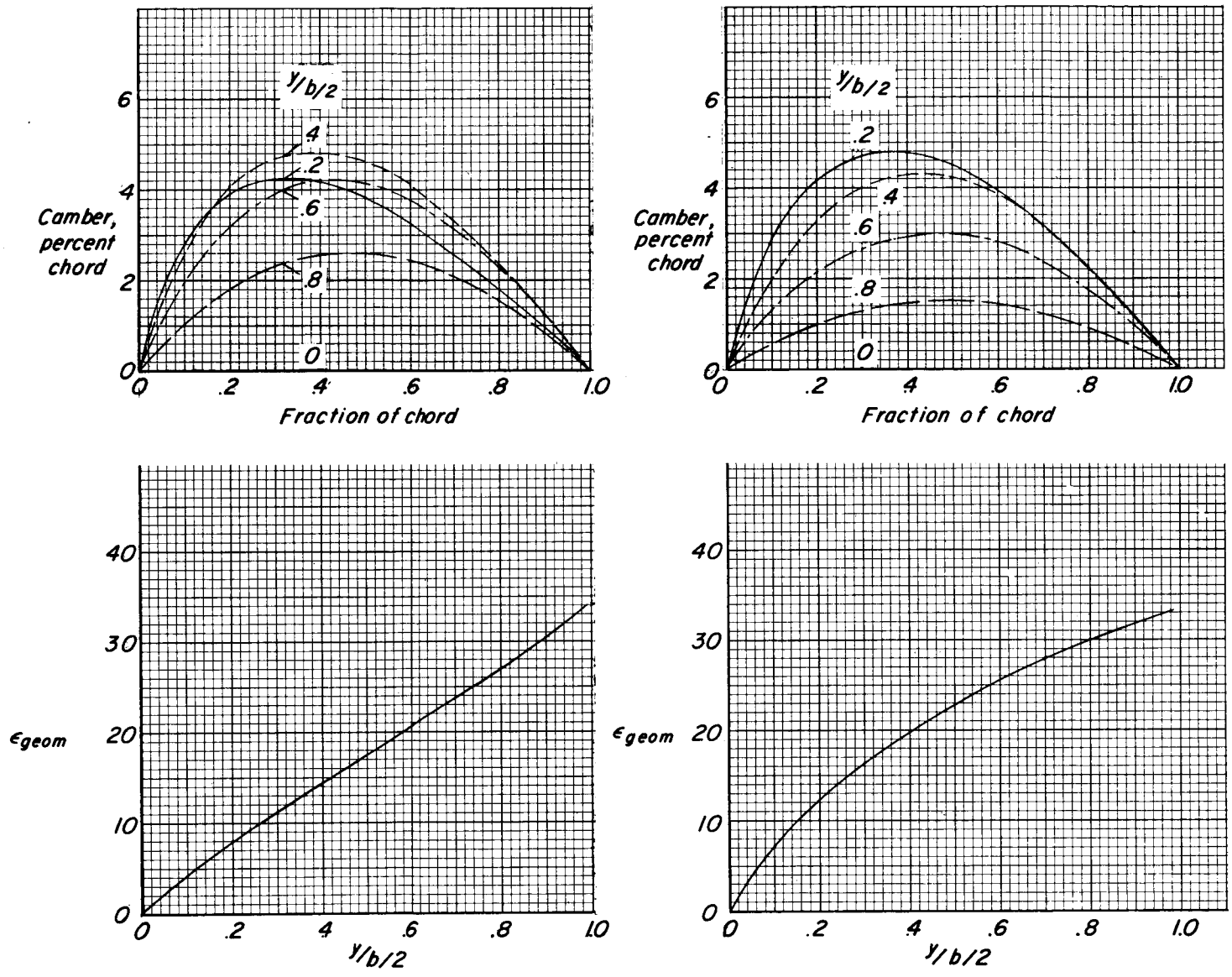

(a) Aspect ratio 3.

(b) Aspect ratio 6.

Figure 9.- Calculated variations of geometric twist and camber. Conical surfaces.

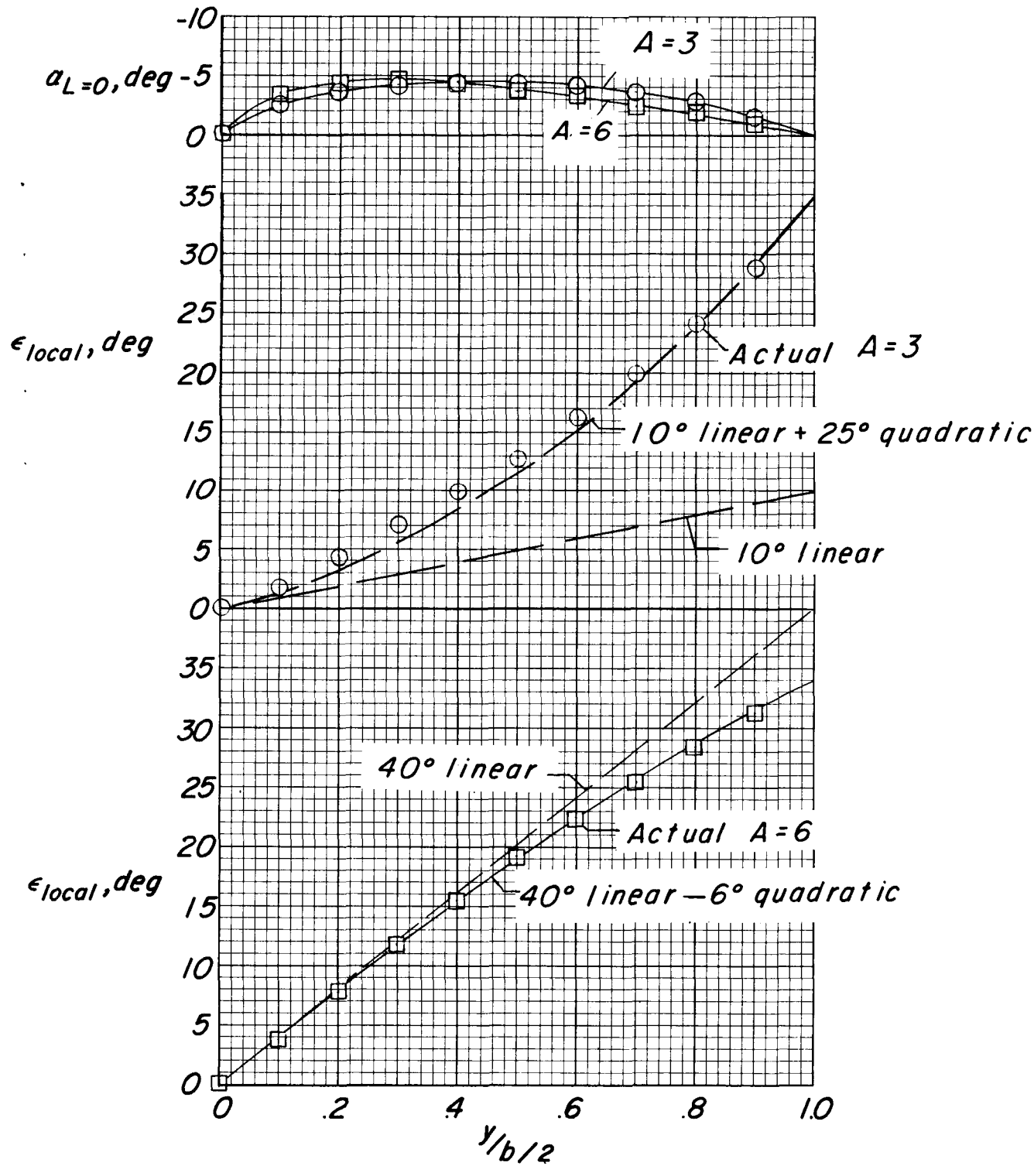

Figure 10.- Theoretical spanwise variation of the angle for zero lift and the net aerodynamic twist. Conical wings.

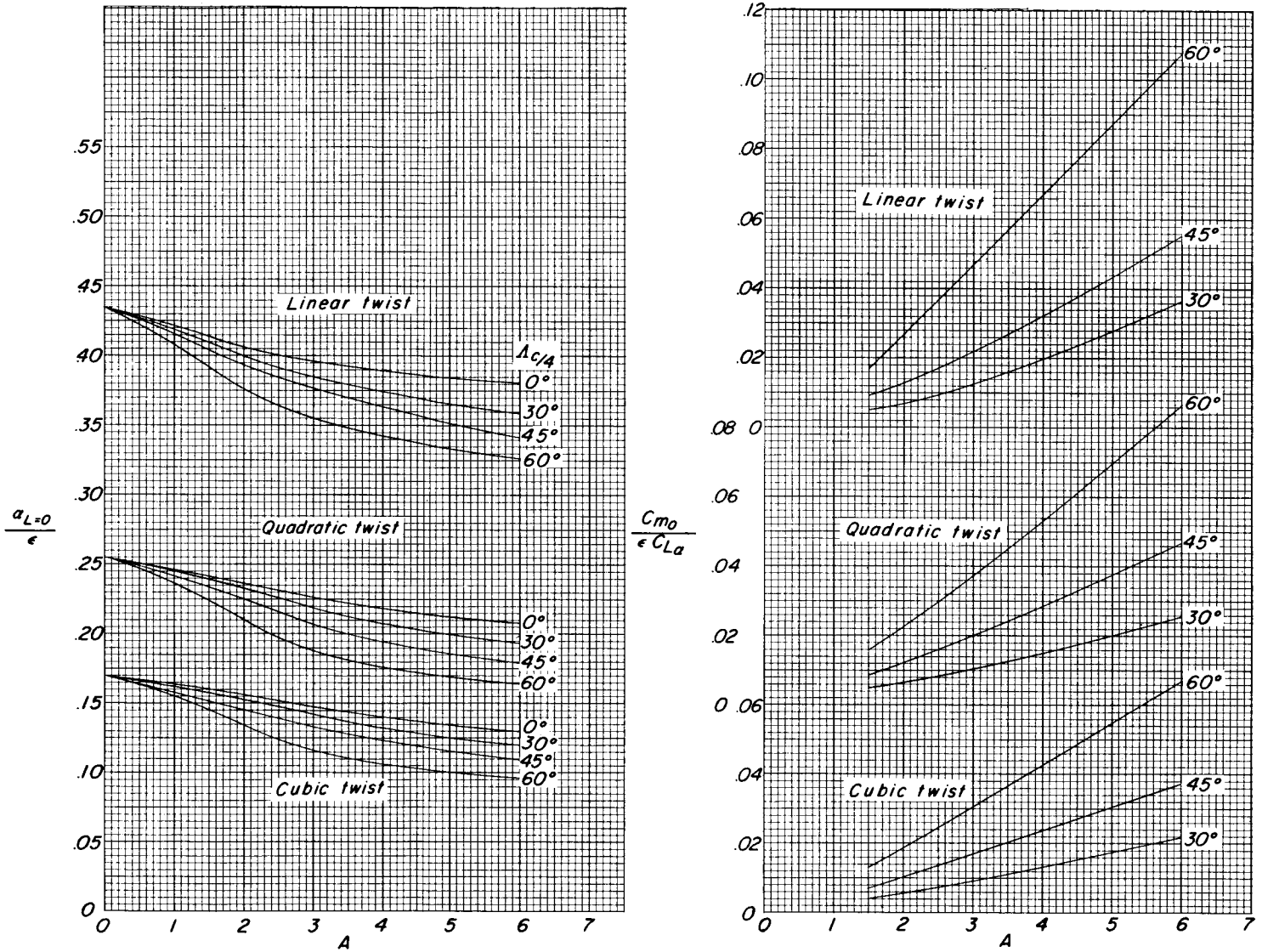

Figure 11.- Theoretical values of $\frac{a_{L=0}}{\epsilon}$ and $\frac{C_{m_o}}{\epsilon C_{L_\alpha}}$ obtained from Weissinger 15-point modified lifting-line span loadings of references 12 and 13. C_{m_o} is based on keel length. Aspect ratios and sweep angles refer to deployed wing.

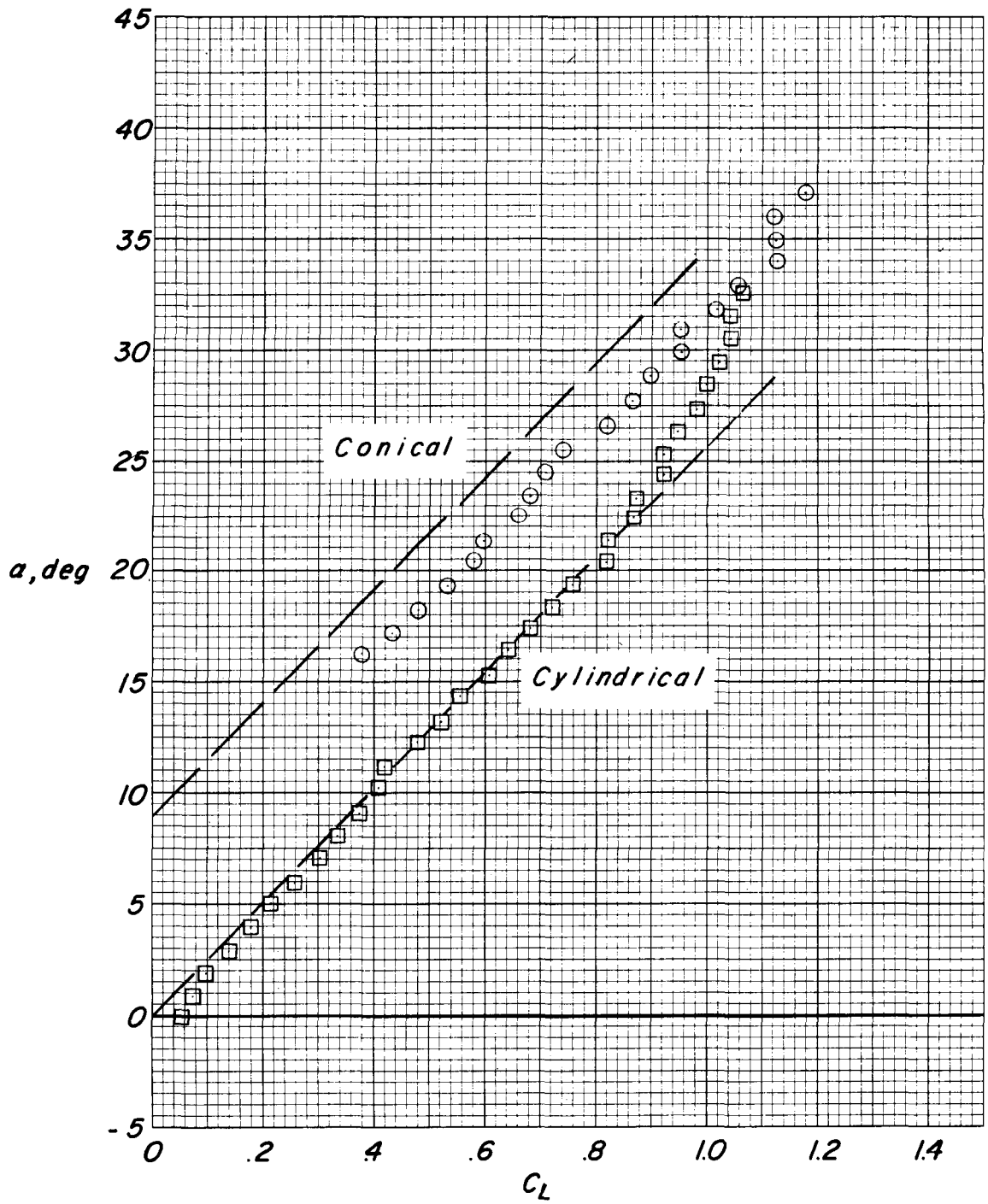

(a) Aspect ratio 3.

Figure 12.- Comparison of estimated and experimental lift characteristics. Theoretical results are shown as dashed lines.

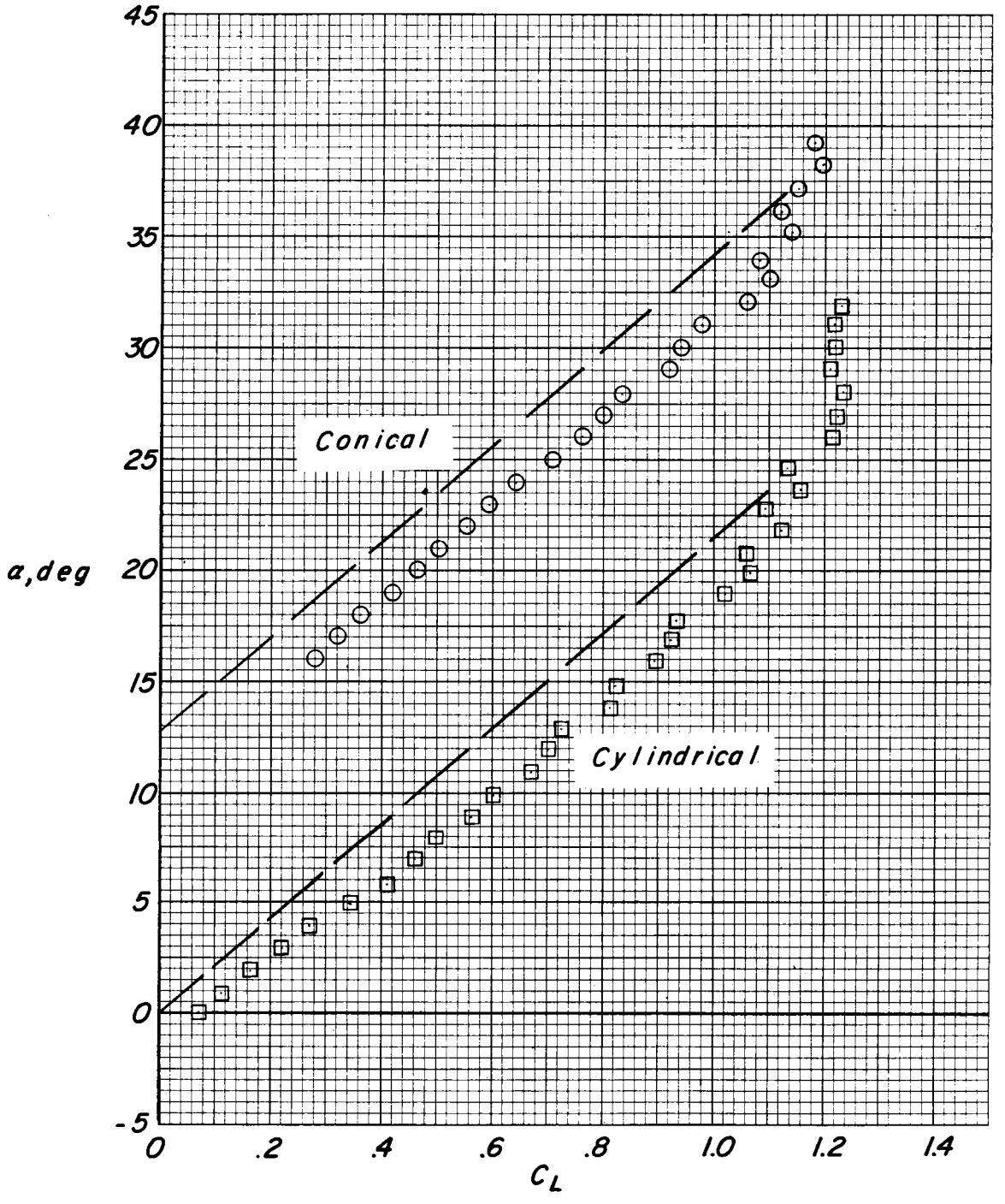

(b) Aspect ratio 6.

Figure 12.- Concluded.

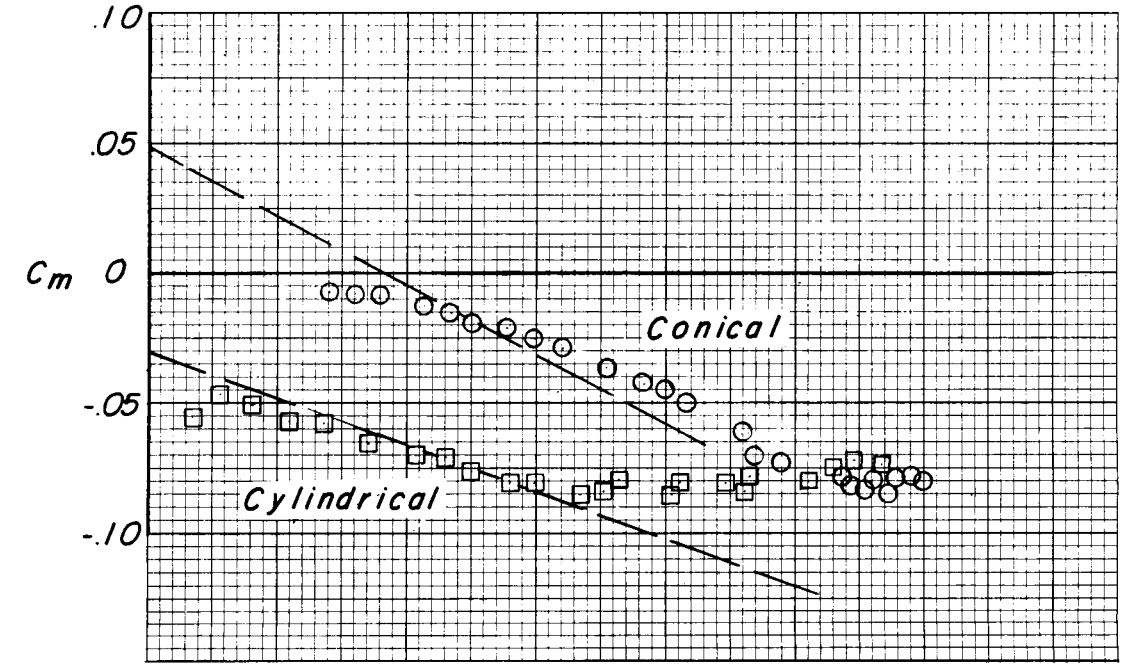

(a) Aspect ratio 6.

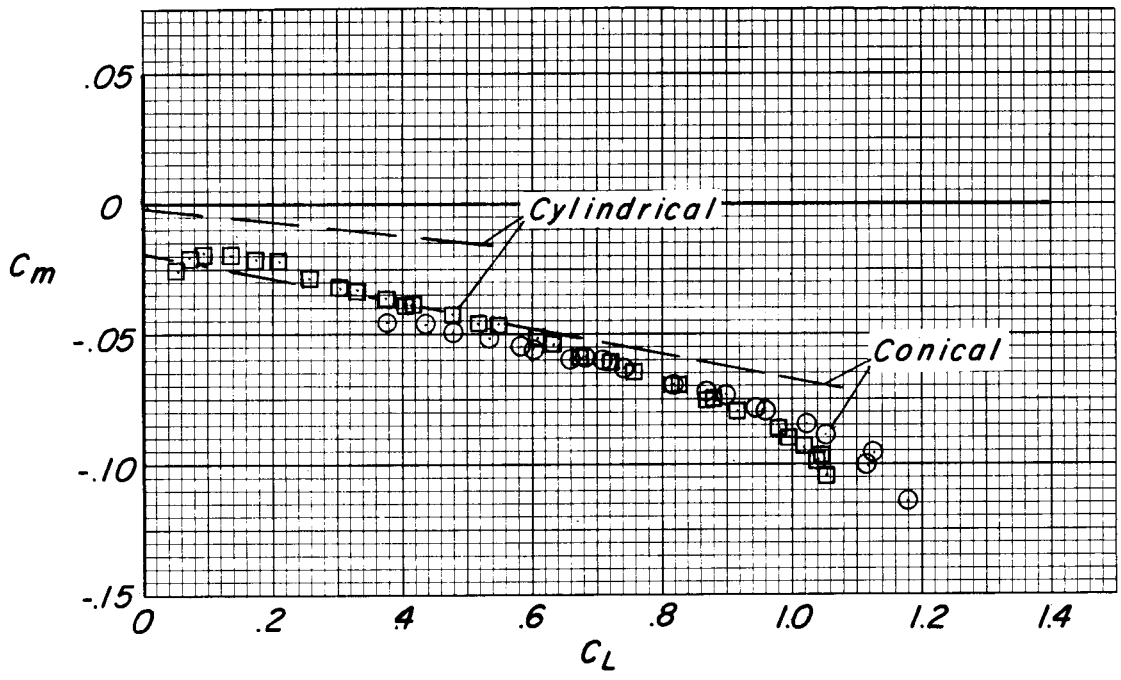

(b) Aspect ratio 3.

Figure 13.- Comparison of estimated and experimental pitching-moment characteristics. Theoretical results are shown as dashed lines.